UCID-15644-77-1

Lawrence Livermore Laboratory

GENERAL CHEMISTRY DIVISION QUARTERLY REPORT

January through March 1977

Scientific Editor: J. E. Harrar

June 24, 1977

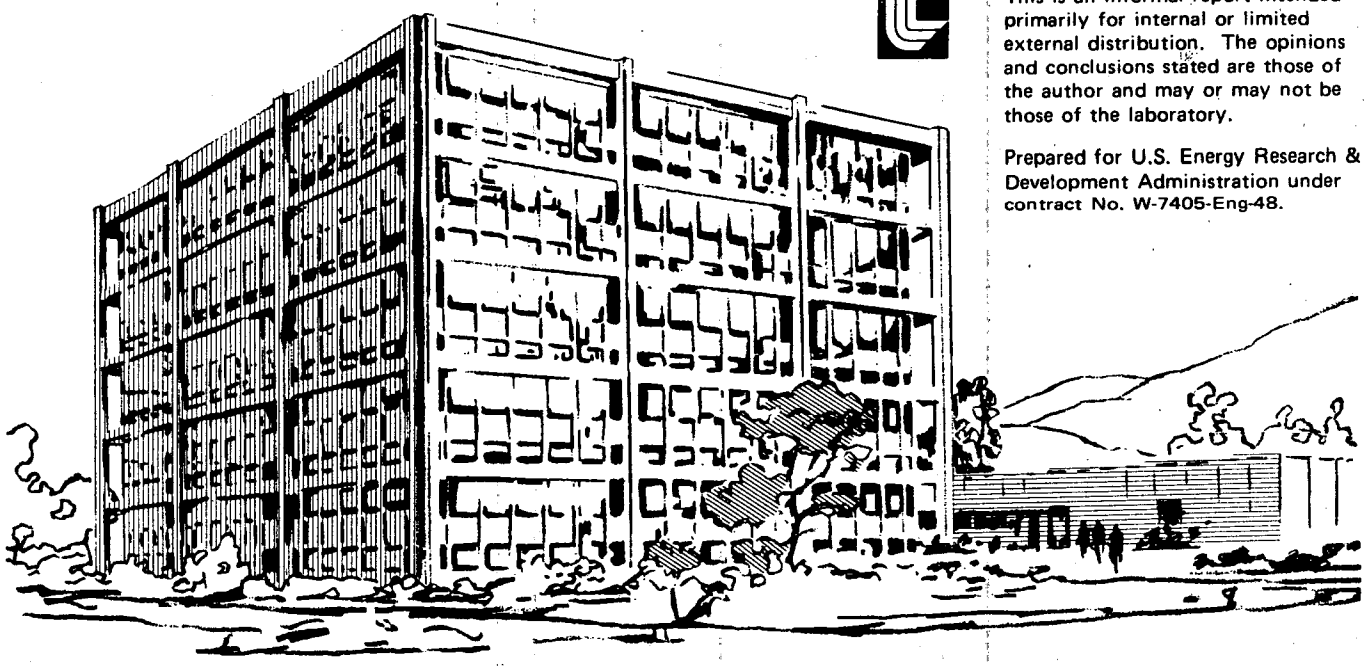

Prepared for U.S. Energy Research & Development Administration under contract No. W-7405-Eng-48.

DISCLAIMER

Printed in the United States of America
Available from
National Technical Information Service
U.S. Department of Commerce
5285 Port Royal Road
Springfield, VA 22161
Price: Printed Copy $; Microfiche $3.00

Page Range	Domestic Price	Page Range	Domestic Price
001–025	$ 3.50	326–350	10.00
026–050	4.00	351–375	10.50
051–075	4.50	376–400	10.75
076–100	5.00	401–425	11.00
101–125	5.50	426–450	11.75
126–150	6.00	451–475	12.00
151–175	6.75	476–500	12.50
176–200	7.50	501–525	12.75
201–225	7.75	526–550	13.00
226–250	8.00	551–575	13.50
251–275	9.00	576–600	13.75
276–300	9.25	601–up	*
301–325	9.75		

*Add $2.50 for each additional 100 page increment from 601 to 1,000 pages; add $4.50 for each additional 100 page increment over 1,000 pages.

CONTENTS

GENERAL CHEMISTRY DIVISION QUARTERLY REPORT

Analytical Research and Development for the Nuclear Explosive Programs

Stark-Shift Laser Spectrometry for Chemical Analysis

Responsible Personnel: L. W. Hrubesh, D. C. Johnson,* M. Revelli, and E. A. Rinehart†

Brief Description: We are continuing to develop a submillimeter laser spectrometer[1] and to characterize its analytical capabilities.

Status: The crude apparatus constructed for the initial investigations in Stark-shift laser spectrometry (SSLS) had significant limitations. Our studies require system stability; the amplitude and frequency stability of the pump laser are particularly critical. We have now designed and constructed a CO_2 pump laser with the necessary stability characteristics. This laser presently is being aligned and tested and will be available as a pump for the submillimeter laser by the end of April.

Our past work in SSLS has been done with a Stark cell that is positioned in the beam of the submillimeter laser[1] but is external to the submillimeter laser itself. If the Stark sample cell were placed inside the submillimeter laser, the sensitivity could be increased in proportion to the increased radiation path length through the gas.

We have completed a design which will facilitate the (intracavity) Stark cell; it is currently being fabricated. The design also incorporates a parallel-plate, submillimeter laser resonator to provide some tunability of the long-wavelength radiation by Stark shifting. This extra capability will be used mainly to ensure better coincidence (and thus higher pumping efficiency) between the CO_2 pump laser wavelength and the submillimeter laser transition wavelength.

---

*Research Engineering Division, LLL.

†Consultant, University of Wyoming, Laramie, Wyoming.

1. General Chemistry Division Quarterly Report, October through December 1976, Lawrence Livermore Laboratory, Rept. UCID-15644-76-4 (1977), p. 18.

It is desirable to predetermine, by calculation, those transitions for polar molecules which have large Stark effects. Such transitions are most easily observed by SSLS. We have obtained a computer program that can perform the desired calculations for a large number of molecules and are currently adapting it to run on LLL computers.

The precise measurement of submillimeter wavelength (or the corresponding frequencies) is difficult. Several laboratories working in this wavelength region use an extension of microwave techniques to measure the frequencies precisely. A recent development at the MIT Lincoln Laboratory under ERDA sponsorship has produced point-contact Shottky diodes that are efficient harmonic mixers in the submillimeter wavelength region. Although these diodes are not yet commercially available, we have been able to obtain one from Lincoln Laboratory. We will be testing this diode in the next few months for use in our spectrometer to precisely measure frequencies.

Laser-Induced Molecular Fluorescence

Responsible Personnel: J. H. Richardson, L. L. Steinmetz,* B. W. Wallin,† and J. C. Bartholomew**

Brief Description: Several biochemically important compounds have been quantitatively detected in aqueous solutions by laser-induced molecular fluorescence (LIMF). Significant improvements in the minimum detectability have been obtained when compared to conventional fluorescence. A fluorescent label was evaluated for use with some of these biochemicals as well as for possible application to explosive detection. In addition, a feasibility study using time-resolved fluorescence has been initiated to determine the kinetics of carcinogen binding to DNA.

Status: LIMF research, a major project of LCA (Lasers for Chemical Analysis), has entered its third and final phase — the detection of biochemicals and explosives. Previous work has demonstrated the sub-part-per-trillion sensitivity of this technique in both the visible[2] and ultraviolet[3] spectral regions.

The biochemical portion of the study has been completed and the results are summarized in Table 1. The use of fluorescamine (Fluram††) as a fluorescent label for primary amines greatly augments the sensitivity of the technique. It also increases the number of compounds that can be studied by LIMF. Aniline and benzene have similar fluorescent characteristics; yet, the minimum detectability of fluorescamine-labeled aniline is more than 1000 times lower than that of benzene.

---

*Electronics Engineering Department, LLL.

†Research Engineering Division, LLL.

**Laboratory of Chemical Biodynamics, LBL.

2. J. H. Richardson, B. W. Wallin, D. C. Johnson, and L. W. Hrubesh, Anal. Chem. Acta 86, 263 (1976).

3. J. H. Richardson and M. E. Ando, Anal. Chem. 49, 955 (1977).

††Reference to a company or product name does not imply approval or recommendation of the product by the University of California or the U.S. Energy Research and Development Administration to the exclusion of others that may be suitable.

Table 1. Limits of detection of biochemicals in water.

Compound	Excitation wavelength (λ_{ex}), nm	Absorptivity at λ_{ex}, $mol^{-1} \cdot cm^{-1}$	Fluorescence wavelength (λ_{em}), nm	Quantum yield	Limits of detection			
					LIMF		Conventional	
					mol	ppb	mol	ppb
Vitamin A acetate	337.1	1.8×10^{4}	500	—	3×10^{-9}	1.0	—	100
Vitamin B_2 (riboflavin)	375.0	1.1×10^{4}	540	0.26	1.25×10^{-12}	0.47×10^{-3}	1×10^{-10}	0.038
FAD	267.0	3.8×10^{4}	525	0.04	5×10^{-11}	39×10^{-3}	—	—
Vitamin B_6 (pyridoxine)	337.1	1.6×10^{3}	410	0.10	2.5×10^{-10}	50×10^{-3}	—	1.5
Vitamin B_{12} (cyanocobalamin)	260.0	1.2×10^{4}	310	—	$\sim 1 \times 10^{-7}$	1.4×10^{2}	—	—
Tryptophan	270.0	5.4×10^{3}	358	0.13	2.5×10^{-10}	50×10^{-3}	—	3
Aniline/Fluram	390.0	1.7×10^{4}	500	0.28	3.8×10^{-11}	3.5×10^{-3}	—	>40
Arginine/Fluram	390.0	$\sim 1.7 \times 10^{4}$	500	~0.25	5×10^{-11}	10×10^{-3}	—	300

The use of fluorescamine as a label for amino acids potentially enhances the minimum detectability of proteins more than tenfold; tryptophan, the most fluorescent amino acid, has a minimum detectability ten times greater than that of fluorescamine-labeled arginine. Of course, the minimum detectability of tryptophan is substantially lowered through the use of LIMF.

No further work is being contemplated for biochemicals. A survey of the fluorescent properties of explosives remains to be conducted. However, it is likely that explosives are poor fluorophors. Some initial experiments indicate that fluorescamine was attached in low yield, if at all, to o-nitroaniline, a nonexplosive analog of TATB. This can be attributed to the decreased nucleophilicity of the primary amine in o-nitroaniline. A drastic increase in the alkalinity of the solution (e.g., by reaction with metal hydride) or a reduction of the nitro groups might alleviate this problem.

Benzo(a)pyrene (BaP), a potent carcinogen, was also studied. It is metabolized through a series of enzymatic reactions to 7,8-diol-4(H)BaP-9, 10-oxide which, in turn, rapidly and covalently bonds to and intercalates into DNA.

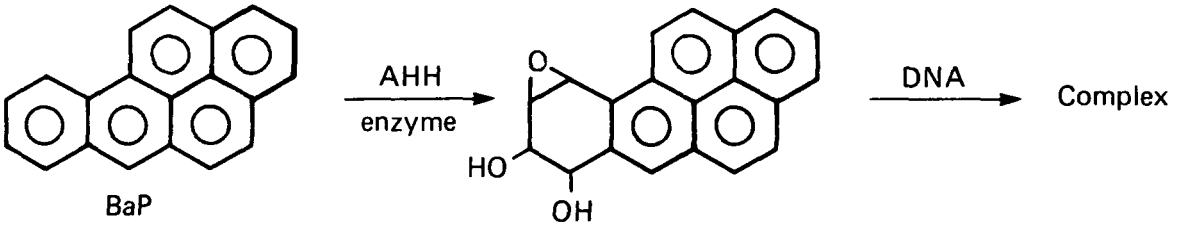

The fluorescent lifetimes of BaP and of the diol-epoxide BaP in hexane solution have been measured using the doubled output of the Molectron dye laser. We found that deoxygenating the solutions greatly enhanced the fluorescent lifetime. The lifetime of pyrene in hexane and in aqueous solutions, both in the presence and absence of oxygen, has also been measured with the Molectron laser and compared to measurements made with the ORTEC instrumentation.[4] Remaining work includes measuring the lifetimes of BaP and the diol-epoxide BaP in water and in the DNA complex as well as obtaining

4. J. H. Richardson, Sensitive Assay of Biochemicals by Laser Induced Molecular Fluorescence, Lawrence Livermore Laboratory, Rept. UCRL-79431 (1977).

good absorption and fluorescence spectra under all the various conditions of interest. It should then be possible to decide whether the DNA binding kinetics can be followed by time-resolved fluorescence.

Laser Photoionization Mass Spectrometry

Responsible Personnel: R. G. Bedford and K. Ernst

Brief Description: The feasibility of using a laser photoionization source for analytical mass spectrometry is being investigated. Literature has been reviewed and the requirements of a useful ion source have been evaluated and compared with the capabilities of commercially available lasers.

Status: Photoionization has a number of characteristics that make it attractive for use in analytical mass spectrometry:

- High temperatures are not required in this source as they are in the emitter in electron bombardment sources.
- It is much easier to obtain a beam with a narrow energy spread with photoionization than it is with electron bombardment.
- Ionization efficiency curves rise more abruptly above the threshold energy.
- Photoion spectra usually show less fragmentation and have more intense parent-ion peaks than do electron impact ion spectra.
- The ionizing beam is electrically neutral.

Because of these characteristics, the following favorable features result:

- Undesired reactions in the source (e.g., the pyrolysis of unstable compounds) can be avoided.
- Accurate ionization and appearance potentials can be measured.
- Selective ionization if more easily achieved.
- Photoion spectra from mixtures usually are easier to interpret than the corresponding electron bombardment ion spectra.
- The ion source can be designed to optimize extraction efficiency and ion focusing.

Disadvantages of photoionization include the fact that ionization cross sections are relatively small, usually about 1% of electron bombardment cross sections. Also, it is difficult to produce narrow-band photon beams with intensities as high as those of electron beams. If broadband radiation is used, many of the advantages of photoionization are lost.

Neither direct photoionization nor multiphoton ionization with laser sources appears to be practical at the present time because of limitations on the energy and power density of available lasers. However, there does seem

to be a good chance that a source with two or more high-power, tunable, ultraviolet pulsed lasers can be developed using a multistep process. Such a source would offer the advantages of low sample decomposition rates, selective ionization, and less complicated spectra that are obtained with photoionization, while retaining a sensitivity comparable to or higher than that available with electron bombardment ion sources.

Only one reference was found in the literature on general purpose laser photoionization sources: a U.S. patent for a "High Brightness Ion Source," by R. W. Dreyfus and R. T. Hodgson (of I.B.M.), U.S. Patent No. 3,914,655 (1975).

Photoacoustic Spectroscopy of Solids

Responsible Personnel: R. G. Gutmacher and J. H. Richardson

Brief Description: An instrument for photoacoustic spectroscopy of solids has been assembled. Cells for holding the sample and a microphone also have been designed and built. Initial experiments have been performed with the instrument.

Status: Photoacoustic spectroscopy (also known as opto-acoustic spectroscopy) can provide an absorption spectrum of any kind of solid except those that are completely opaque (e.g., graphite). In photoacoustic spectroscopy of solids,[5-7] the sample to be studied is placed inside a closed chamber, the photoacoustic cell. This cell is filled with a gas, such as air, at room temperature and pressure. The cell also contains a very sensitive microphone. The sample then is illuminated with chopped monochromatic light. If the sample absorbs any of the incident radiation and de-excitation takes place in a nonradiative or heating mode, a periodic heating of the sample occurs with a subsequent periodic heat flow from the sample to the surrounding gas. This translates into a periodic pressure change in the cell that is detected by the microphone as an acoustic signal.

The strength of the acoustic signal is closely related to the amount of light absorbed by the sample. Thus, a photoacoustic spectrum, obtained by plotting the acoustic signal vs the wavelength of the incident light, bears a close resemblance to a true optical absorption spectrum. In theory, only absorbed light can produce an acoustic signal. Hence scattered light, which presents a serious problem in conventional absorption spectroscopy of solids, should not interfere in photoacoustic spectroscopy. Because this technique is applicable to solids of all kinds, it should be widely applicable to the study of materials problems.

We have constructed an instrument for photoacoustic spectroscopy of solids (see Fig. 1). The tunable light source may be a cw dye laser or a

---

5. A. Rosencwaig, Anal. Chem. 47, 592A (1975).
6. M. J. Adams, A. A. King, and G. F. Kirkbright, Anal. 101, 73 (1976).
7. J. F. McClelland and R. N. Kniseley, Appl. Optics 15, 2658 (1976).

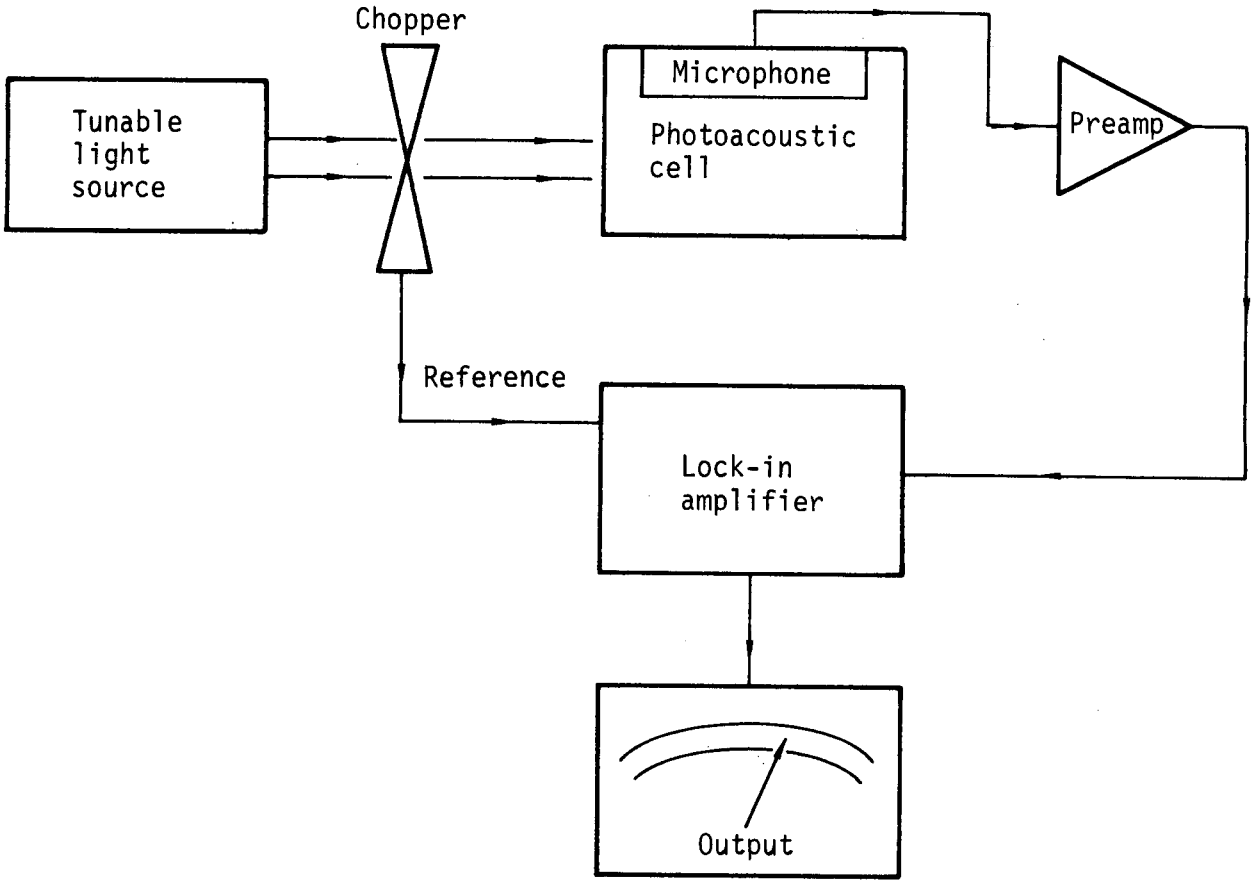

Fig. 1. Diagram of a single-beam photoacoustic spectrometer.

high intensity xenon lamp combined with a scanning monochromator. The photoacoustic cell was designed by us and built to our specifications. The microphone is a very sensitive 2.5-cm-diameter condenser or electret microphone. We found it necessary to build a suspension for the photoacoustic cell and mount the mechanical chopper independently of the optical table to eliminate vibrational interference.

In our initial experiments, we used a cw dye laser with Rhodamine 6G as the dye for the tunable light source. When finely powdered graphite was used as the sample and the laser scanned over the lasing range of the dye, we obtained a photoacoustic spectrum that corresponds to the power spectrum of the laser. We also obtained photoacoustic spectra for some less opaque compounds, such as Cr_2O_3, that had been studied by previous investigators. In future experiments, we will use a recently received 1000-W xenon lamp and the scanning monochromator to rapidly record photoacoustic spectra over a wider spectral range than is conveniently possible with the dye laser. The dye laser will be valuable in situations where high sensitivity of detection is required at a particular wavelength.

Time-Resolved Spectroscopy

Responsible Personnel: G. R. Haugen, F. E. Lytle,* B. W. Wallin,† L. L. Steinmetz,** D. C. Johnson,† and J. D. Breshears**

Brief Description: Analytical utilization of photoluminescence would be enhanced by time resolution of the process because all of the information contained in the luminescence can, in principle, be recovered. Multicomponent mixtures may be analyzed with this technique. To study the potentials of this technique, we have assembled and tested a time-resolved fluorimeter that uses a pulsed laser source and single-photon counting techniques.

Status: Luminescence spectrometric techniques are among the most sensitive analytical methods for trace analysis. However, the majority of the fluorimetric methods for analysis have utilized steady-state luminescent techniques involving observations of either the spectral content (emission and excitation spectra) or of luminescent quenching. Until recently, transient fluorimetry was not used extensively as an analytical tool. This technique is becoming increasingly important, especially in the fields of biochemistry and biology.

Previously, transient luminescence measurements required the use of a wide spectral bandwidth with a concordant loss in information. High-resolution, time-resolved spectroscopy now is feasible with state-of-the-art sophisticated, pulsed, light detection techniques such as time-correlated, single-photon counting and pulsed radiation sources such as pulse-picked, mode-locked lasers.

Time-resolved spectroscopy can enable a significant improvement in the sensitivity and selectivity of analytical measurements by rejecting interfering background luminescence signals. The enhancement of Raman emission from an intensely luminescent background by temporal rejection of that background has already been demonstrated. Conversely, the limit of detectability of fluorescence can be enhanced by temporal rejection of scattered emission and

---

*Purdue University, Lafayette, Indiana.

†Research Engineering Division, LLL.

**Electronics Engineering Department, LLL.

reagent luminescence. The potential analytical utility of time-resolved fluorescence is great because, in principle, all of the information contained in the signal (e.g., spectral behavior, polarization, quantum efficiency, and decay behavior) can be recovered. Multicomponent systems could be analyzed by a differential kinetic analysis of the time- and wavelength-evolution of the intensity of fluorescence emitted by such systems.

The apparatus assembled for studying time-resolved fluorimetry is shown in Fig. 2. Pulses from the PIN diode enter the discriminator, which times the excitation of the sample. The shape and amplitude of the PIN diode pulse are extremely stable; consequently, this discriminator uses leading-edge timing to originate a start pulse for the time-to-amplitude converter (TAC). The sample emits a fluorescent photon which is transformed into a single-photoelectron pulse by the photomultiplier. The anode pulse is fed to a discriminator after amplifying and shaping. Although the shape of the anode pulses are invariant, their amplitude fluctuates. To eliminate the timing jitter, this discriminator uses constant-fraction time to originate a stop pulse for the TAC.

The TAC outputs a square pulse; the pulse height is proportional to the time that elapsed between the start and stop pulses. The number of occurrences in each time channel is accumulated in the multichannel analyzer (MCA), by determining the height of the TAC pulse and converting it to a digital address. An internal analog-to-digital converter in the MCA performs this conversion.

The counting statistics of this measurement can be distorted if the separation time between photoelectron events is smaller than the processing and recovery time of TAC and MCA. To prevent such distortions from occurring at high data acquisition rates, two precautions are necessary. First, the number of photons arriving at the photocathode of the photomultiplier is attenuated to the point where the multiphoton events are a small fraction of the total events. Second, a window is selected to delineate single-photoelectron events and reject all events outside of this window.

Photocathode events separated by more than the transit time of the photomultiplier will produce separate single-photon pulses at the anode. These can cause a pulse pile-up error at the TAC. This error can be effectively eliminated by observing the photoelectron pulses at the last dynode with an amplifier that scans the electron cascades of pulses arriving within the recovery time of the amplifier. The amplitude of the amplifier pulse is examined to determine if it is in or out of the bounds of this window. Next,

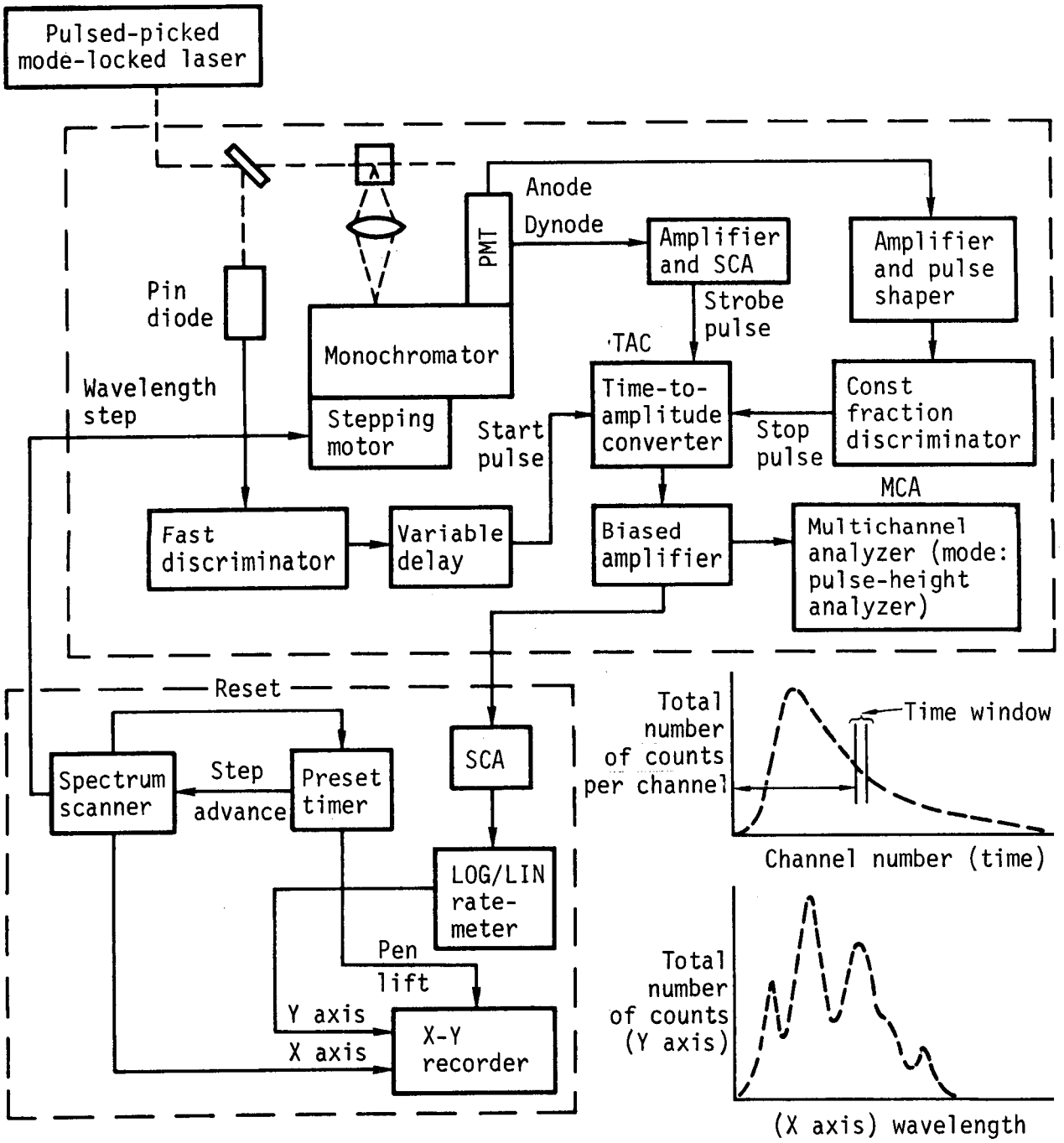

Fig. 2. Diagram of the time-resolved fluorimeter.

a logic pulse decides whether or not to strobe the pulse height information to the MCA.

The emission spectrum at a selected time window after excitation can be obtained with a single-channel analyzer (SCA) that selects the appropriate TAC output pulses. A linear rate-meter integrates these pulses and outputs an analog signal to the Y axis of the X-Y recorder. This analog signal is proportional to the fluorescent intensity at the specified wavelength and time window. After a preset time, the spectrum scanner advances the monochromator and the X-Y recorder to a new wavelength where the linear rate-meter begins measuring the fluorescent intensity. Accordingly, the emission spectrum can be established over any time window.

The emission enhancement obtained by switching from a continuous to a time-resolved experiment is a function not only of the window in which the photons are accepted but also of the position of the sample time and the temporal behavior of the different emission. However, the signal-to-noise ratio for a time-resolved experiment deteriorates over that for continuous excitations. This deterioration is due mainly to the reduction in the average power incident on the sample.

Improvement of the signal-to-noise ratio requires faster repetition rates. The repetition rate is limited by the photon counting circuitry. It is not limited by the repetition rate of the laser because mode-locked, cavity-dumped argon ion lasers have an average power that rolls off at approximately 4 MHz. The time-correlated, single-photon technique provides a slower data-acquisition rate than is available with many of the other techniques. To date, this has not been important because the data-acquisition rate has been restricted by the slow repetition rate of the excitation source (gas discharge lamps). The development of pulsed lasers with high repetition rates has removed this restraint.

Analytical application of time-resolved spectroscopy necessitates the use of fast data-acquisition rates to obtain the highest signal-to-noise ratio in the shortest real time. The keys to the time-correlated, single-photon counting circuitry are the time-to-amplitude converter and the multichannel analyzer. The data-acquisition rate was optimized by operating the TAC in an inverted configuration (see Fig. 3) and by having the busy signal of the TAC control the laser repetition rate. There was a substantial increase in TAC efficiency with this configuration (Fig. 4). Under these conditions,

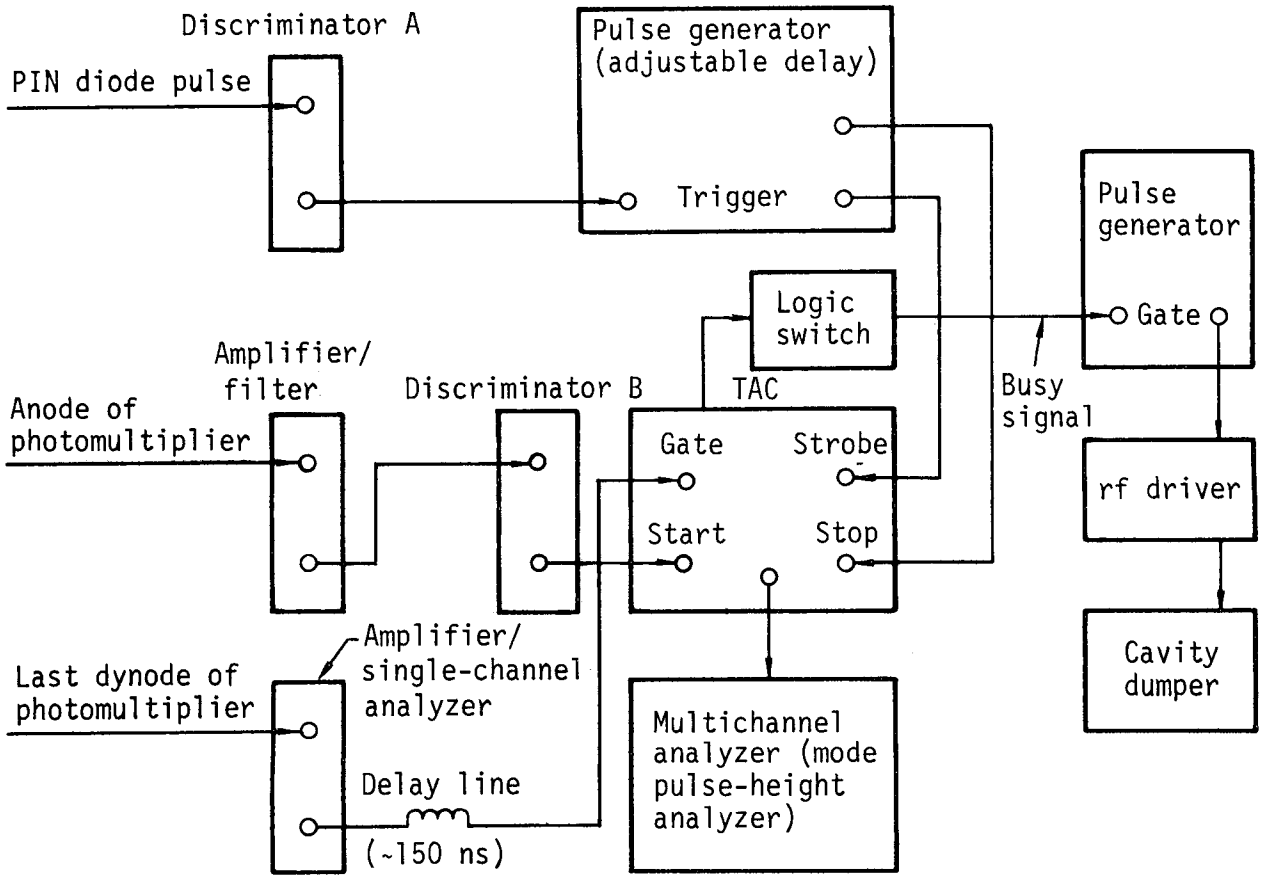

Fig. 3. Diagram of the time-to-amplitude converter in the inverted configuration controlling the cavity dumper.

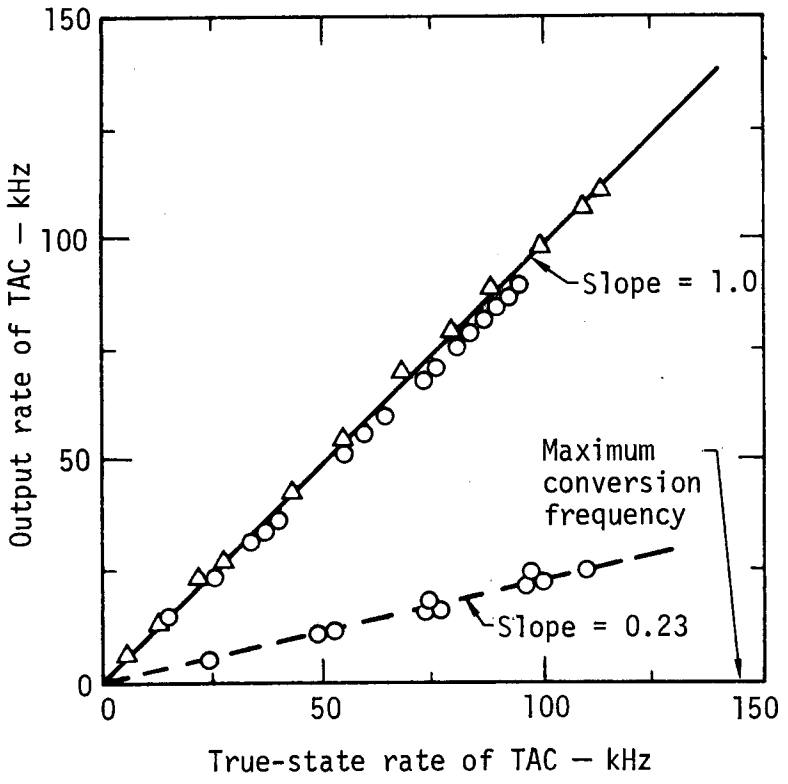

Fig. 4. TAC output for fluorescence of chelate sample for different modes of laser control. The solid curve (slope = 1.0) denotes the TAC in the inverted configuration. The dashed curve (slope = 0.23) denotes the TAC in the normal configuration. The triangles represent scatter radiation from a pure water sample. The circles represent fluorescent radiation from a chelate sample.

the peak-height analyzer in the MCA is the slowest component. A microprocessor has been designed and is under construction to replace this unit.

A new cell compartment also has been designed and is being built. This compartment will increase the optical collection efficiency and decrease the response time of the photomultiplier by illuminating only a small region of the photocathode. Also, it will perform real-time subtraction of background, automatically compare unknown, blank, and standard samples, and enable front-surface observations.

The operation of the system was characterized and two experimental artifacts have emerged. Signal distortion due to finite instrument response and single-photon multiple-pulsing of the photomultiplier are troublesome features. The instrumental output will approach the impulse fluorescence decay function as the instrumental response function approaches the delta function. Typically, the response of the electronics is less than 50 ps and the response of the photomultiplier is a few subnanoseconds. Hence, the excitation source must generate subnanosecond pulses to allow the direct observation of fast fluorescent decays without the need for deconvolution.

Experiments that satisfy this requirement were performed at Purdue University to characterize the operation of a pulse-picked mode-locked argon ion laser. At LLL, the Lexel argon ion laser was modified and successfully mode-locked with its blue and green lines to a pulse width of 250 ps and a repetition rate of 120 MHz. The electronics for the pulse-picker were designed and constructed, but testing and debugging has not yet been completed. Development is continuing to obtain mode-locking in the near ultraviolet.

The other prominent experimental artifact involves the prepulsing and after-pulsing (echo pulse) of the photomultiplier. Prepulsing is caused by photons coming through the photocathode and striking the first dynode. This can be eliminated by illuminating a small area off the center of the photocathode. The cause of the echo pulse is not known and is still being characterized.

A paper detailing this work was presented at the 1977 Pittsburgh Conference on Analytical Chemistry and Applied Spectroscopy and a manuscript is being prepared for journal publication.

Use of Correlation Analysis in Fluorescence Experiments

Responsible Personnel: G. R. Haugen, G. M. Hieftje,* J. M. Ramsey,* and L. L. Steinmetz†

Brief Description: Work is continuing on the use of laser mode noise to obtain measurements of decay curves in fluorescence experiments and to measure the frequency responses of spectral detectors.

Status: The excitation of a fluorophore by rapidly varying fluctuations in a free-running argon ion laser has been shown to produce variations in measured fluorescence. The power spectrum of the fluctuations yields luminescence lifetime information by the use of deconvolution techniques.[8] We have demonstrated the feasibility of this approach using the green 514-nm line of the argon ion laser. We are now attempting to extend the applicability of this approach by frequency doubling the argon ion laser radiation. Use of the 257-nm line would not only enable us to probe many more fluorophores but also would increase the noise amplitude in the exciting radiation, thereby simplifying the necessary noise spectral measurements.

We also have used this technique with the argon ion laser and the helium-neon ion laser to measure the frequency responses of several photodetectors: a Spectra-Physics PIN diode, a Sylvania cross-field photomultiplier, a specially-wired RCA No. 1P28 photomultiplier, a Hewlett-Packard No. 4220 diode, and a Tropel photodiode. These data are being analyzed and prepared for publication.

---

*Indiana University, Bloomington, Indiana.

†Electronics Engineering Department, LLL.

8. G. M. Hieftje, G. R. Haugen, and J. M. Ramsey, Appl. Phys. Lett. 30, 463 (1977).

Excited-State Chemistry of Metal/Oxidant Reactions

Responsible Personnel: M. A. Revelli and D. C. Johnson*

Brief Description: A flow system has been constructed to study the reaction of metal atoms with various oxidants to produce a chemiluminescent flame. Preliminary experiments are in progress to examine the excited-state reaction of Ba^+ (metastable) + $N_2O \rightarrow BaO^* + N_2$.

Status: Laser-induced atomic fluorescence is a sensitive technique for detecting low concentrations of the reactants, intermediates, or products in a chemiluminescent flame. Both the nature and energy state of many reaction species can be determined through the broad-range tunability and narrow bandwidth afforded by dye lasers. Simultaneously, the chemiluminescence spectrum resulting from the reaction can be used to monitor the distribution of product molecules. All of these measurements can be used to probe the overall reaction mechanism.

For these experiments, a vacuum system to house both the furnace assembly and the reaction chamber has been constructed from 10-cm-outside-diameter stainless steel tubing with O-ring flange fittings. Gas inlets, electrical connections, and pressure gauges are introduced through ceramic or O-ring-type feedthroughs. A schematic diagram of the apparatus is shown in Fig. 5. The reaction zone is viewed through three quartz windows and laser radiation enters the chamber vertically through another quartz window at Brewster's angle located above the flame. A particle filter and a throttling valve separate the vacuum system from a bank of mechanical pumps. Operating pressures ranging from 7 Pa to 4 kPa are measured with a 1000-Torr Baratron transducer.

Metal vapor is produced within the furnace assembly by resistively heating the solid in an alumina crucible to approximately 1500 K. The vapor is entrained in an inert carrier gas, injected beneath the crucible, and swept into the reaction chamber through a 0.5-cm aperture in the blackbody radiation shield that surrounds the furnace. The intensity, spectrum, and geometry of

*Research Engineering Division, LLL.

the resulting chemiluminescence depend strongly on the nature of the reactants, their relative concentrations, and the total reaction-zone pressure.

The next milestone for this study of the overall reaction mechanisms is a comparison of chemiluminescence spectra resulting from ground-state vs excited-state reactants for selected metal/oxidant reactions.

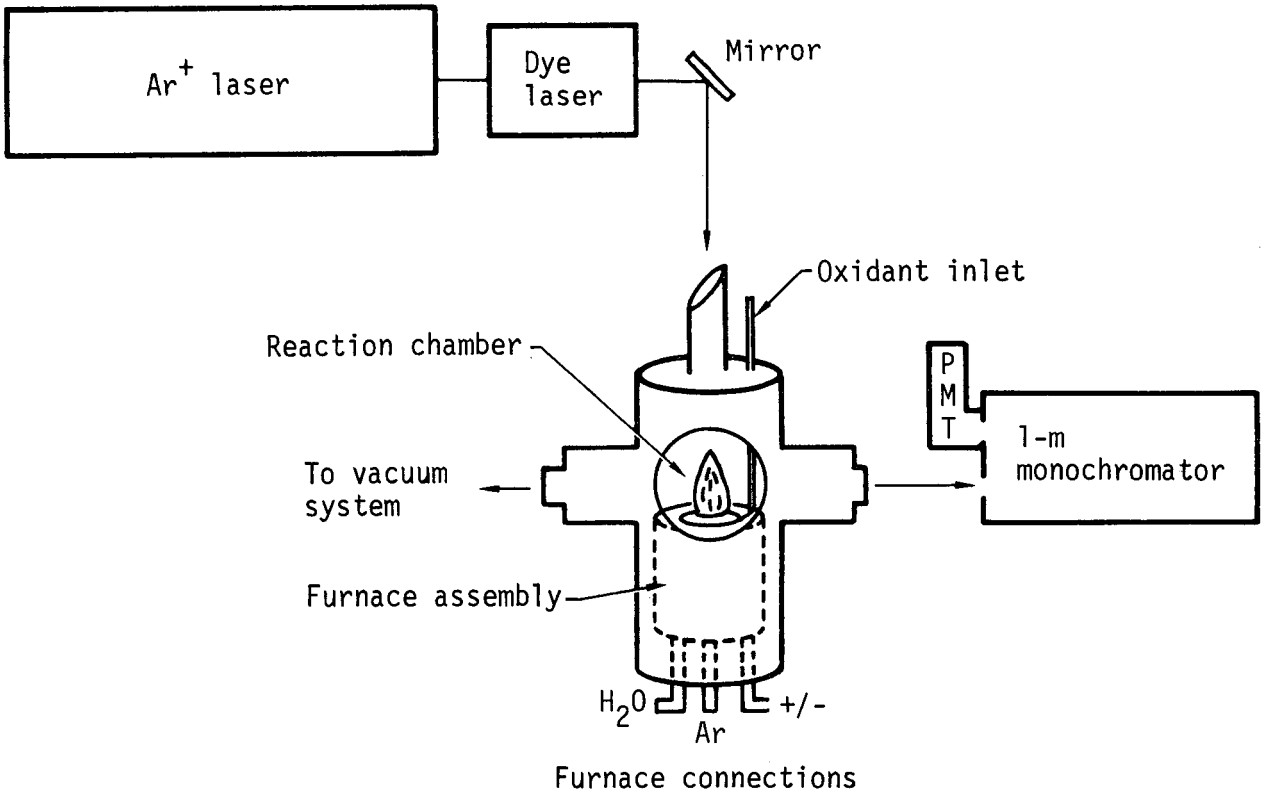

Fig. 5. Apparatus for studying the excited-state chemistry of metal/oxidant reactions.

Ion-Cyclotron-Resonance Mass Spectrometer

Responsible Personnel: R. K. Stump, J. H. Richardson, R. T. McIver,* J. D. Breshears,† and R. S. Hodge**

Brief Description: A new ion-cyclotron-resonance (ICR) spectrometer is being developed[9] that will be versatile and have the capabilities of chemical ionization for the analysis of low-volatility compounds, analysis of low-mass ions, and application to studies of the spectrometric properties of ions.

Status: The primary purpose of this research effort is to construct and evaluate ICR spectrometry for quantitative low-mass analysis (H,D,T, and He). The basic ICR spectrometer has been assembled and testing has been under way for the past several months. The source has been modified for a greater gas flow and a more efficient filament has been built and tested. Programming of the MCS-80 microcomputer that controls the system is almost completed; the program is working and only minor changes must yet be made. A newer version of the program currently is being written for the data-gathering procedure. The vacuum system and the electronics have been mated and are working well under computer control. All valves are electrically controlled and can be operated under computer control.

The computer/operation interaction format used in the system is similar to that of other mass spectrometric techniques. In operation, the computer asks for all voltages to be applied to the cell, the resonance frequencies to be scanned, and the number of repetitions at each frequency. Then, on command, the computer runs each frequency, summing values for each species that is detected and printing out that total. The operator can select either a running total or a separate total for each sweep. The computer generates the time base and applies the appropriate required voltages for generating, separating, and measuring the ions.

---

*University of California, Irvine, California.

†Electronics Engineering Department, LLL.

**Research Engineering Division, LLL.

9. General Chemistry Division Quarterly Report, October through December 1975, Lawrence Livermore Laboratory, Rept. UCID-15644-75-4 (1976), p. 5.

Results of preliminary tests indicate that insufficient resolution was obtained in the analysis at mass 4 (^{4}He and D). We believe this was caused by an undesirably high level of residual gas in the analyzer part of the spectrometer. Collisions of the ions to be detected with molecules of the residual gas increase the background signal and reduce the resolution.

A new faster vacuum pump of a cryogenic type was obtained (see Fig. 6). It operates at liquid helium temperatures and the pressure obtained should be in the range of 10^{-8} Pa. However, this pump is only a temporary solution to the residual gas problem; a turbomolecular-type pump will be used ultimately. The only gas not removed by the cryogenic pump will be helium, which can be removed by the existing pumping package. The present cryogenic pump should reduce the pressure to a point where the ions generated will not collide with a neutral until the ion has been analyzed. When the cryogenic pump is completed and installed, testing and evaluation of the ICR system will continue.

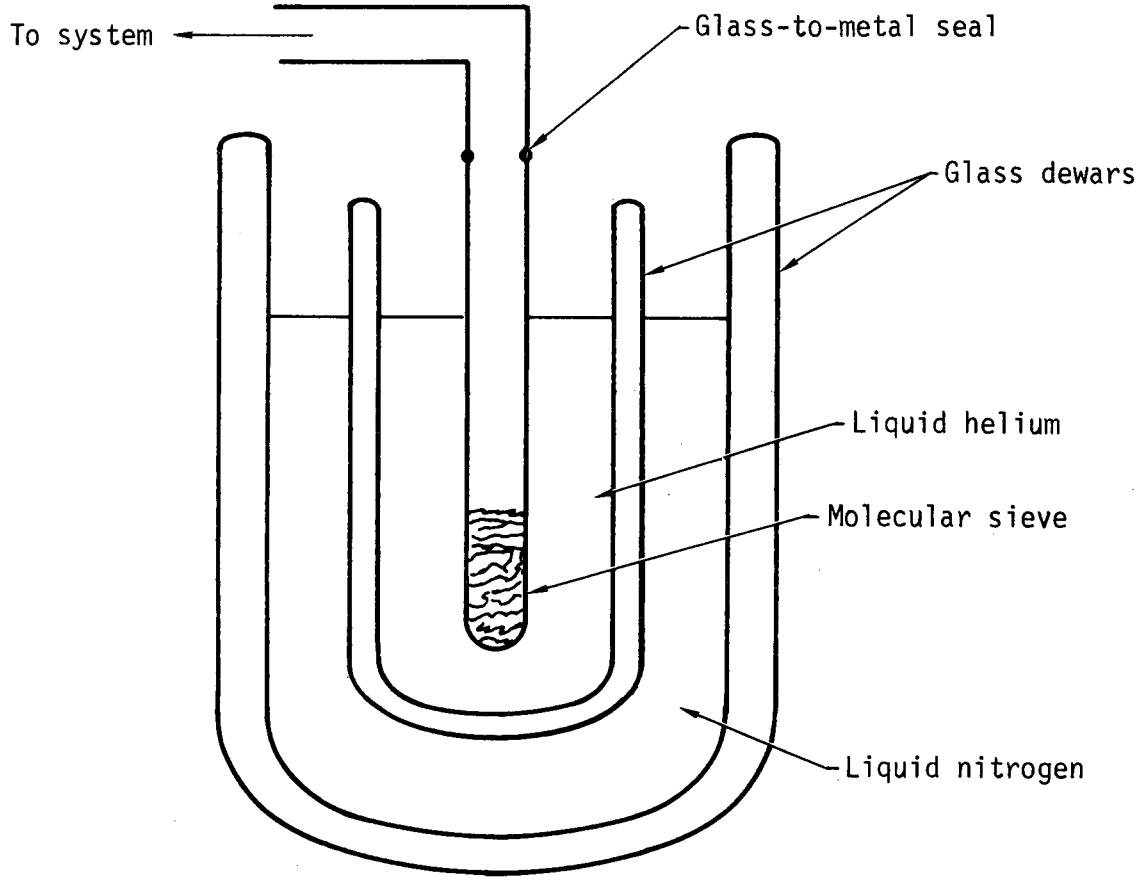

Fig. 6. Cryogenic pump for the ICR system.

Development of Multielement Analysis Systems

Responsible Personnel: R. I. Bystroff and L. R. Layman,* C. L. Pomernacki,† and J. R. Elliott†

Brief Description: An atmospheric glow discharge between tungsten electrodes has been improved and characterized for its possible use as an atom source for multielement spectroscopic analysis.

Status: The atmospheric glow discharge atomizer, first described by Layman and Hieftje,[10] is known to effectively and rapidly atomize small samples (<1 μg) for highly sensitive analytical detection of numerous elements. Typically, picogram detection limits are achieved. We are studying this technique for possible use in a multielement spectroscopic analyzer. To achieve reproducible results, we have chosen first to characterize the source and to qualitatively understand the atomization process.

The discharge is maintained by a full-wave or half-wave ac voltage and is operated between two 0.25-mm-diameter tungsten electrodes in argon at pressures up to 100 kPa (1 atm). To study the cycle-by-cycle operation of this process and to enable control of the electrode temperatures, a power supply controller providing for variable duty cycle operation was designed and constructed. The electrodes were mounted in a vacuum chamber into which controlled quantities of gases could be introduced.

Preliminary spectroscopic observations of the discharge established the importance of residual oxygen to the composition of the cathode sheath. In the entrance, the presence of oxygen leads to rapid erosion of the electrodes and to a plasma characterized entirely by tungsten spectral emission. The addition of 1% hydrogen effectively reduces the effects of residual oxygen, producing a stable, reproducible glow characterized by argon emission. We measured the effective excitation temperature of the cathode sheath by the slope method[11] and found it to be about 5000 K. The degree of scatter obtained is indicative of a lack of thermal equilibrium.

---

*Pacific Lutheran University, Tacoma, Washington.

†Electronics Engineering Department, LLL.

10. L. R. Layman and G. M. Hieftje, Anal. Chem. 47, 194 (1975).

11. I. Rief, V. A. Fassel, and R. N. Kniseley, Spectrochim. Acta 28B, 105 (1973).

Time and spatial information about sample atomization was obtained through the use of both high-speed, motion color photography and linear photodiode arrays with interference filters. In each case, a temporal resolution of a few milliseconds was obtained. The photodiode arrays reveal the spatial distribution of atoms, while the motion pictures demonstrate the dynamics of the vaporizing sample, primarily through the white recombination spectra and the characteristic colors of the metal oxide emission. The combined data are now being analyzed and it is clear that two processes dominate the sample discharge:

- Atomization occurs by argon ion sputtering from a cold electrode.
- Recondensation onto the electrodes, during the period when the discharge is off, plays an important role in the time required for complete atomization and in the spatial distribution of atoms during the course of the discharge.

The evidence for these processes is illustrated in Fig. 7. Here, aluminum emission is observed in the first few milliseconds of the discharge, while the cathode is cold; the temporal behavior of the aluminum signal is consistent with the observed changes in the emission pattern around the electrodes.

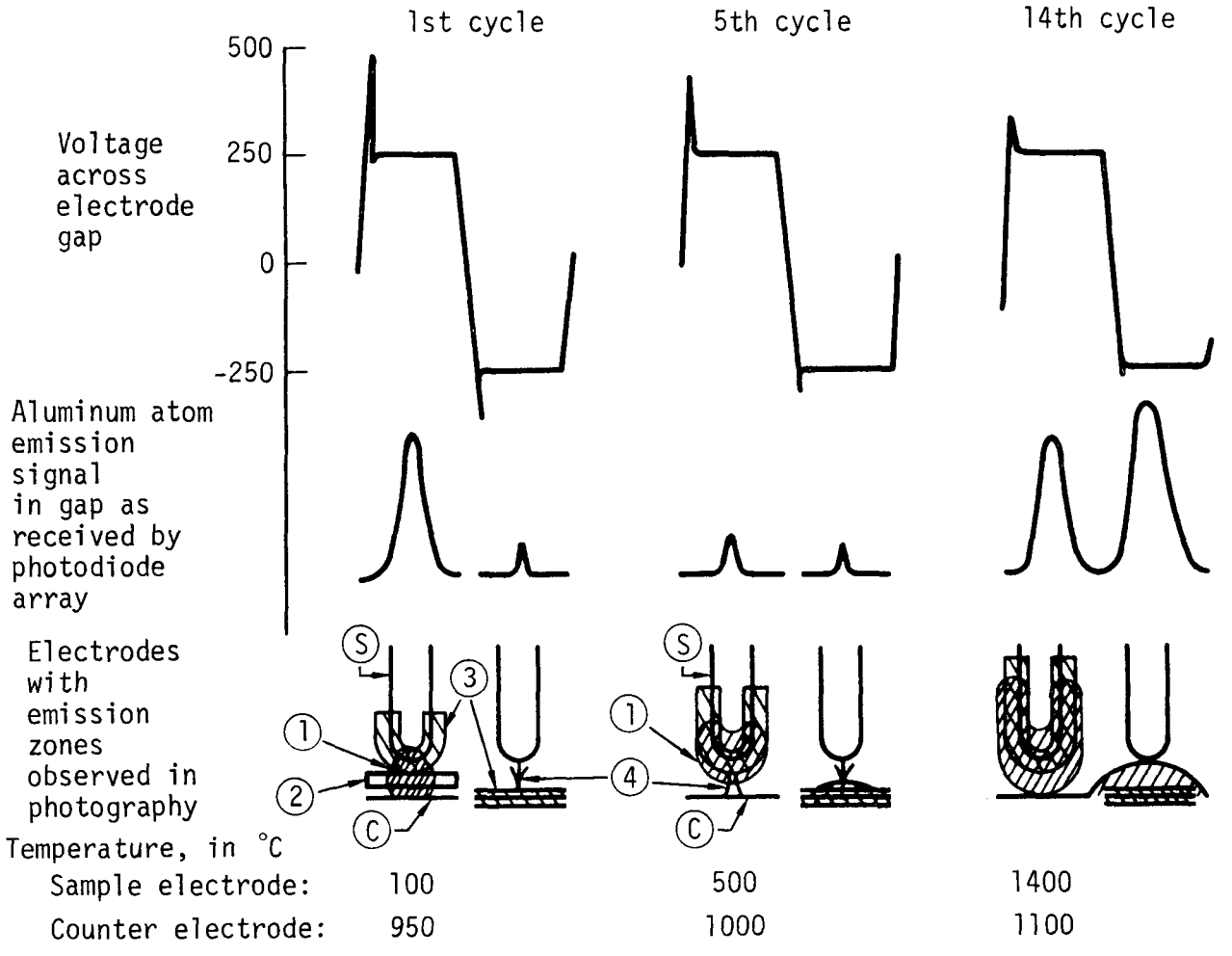

Fig. 7. Diagram illustrating the atmospheric flow discharge as a function of 60-Hz discharge periods and observed signals. The gap voltage (top) shows a decrease in the breakdown overvoltage as the electrode temperature rises and the voltage plateau, characteristic of the glow discharge. The aluminum emission intensity (middle) observed in the region seen by the photodiode array between the electrodes illustrates the drop in emission in the fifth cycle due to redistribution of the atom cloud outside the viewing zone. Diagrams of the electrodes (bottom) illustrate the changing glow discharge and the molecular emission (shaded areas) with increasing time. The emission from the counter electrode becomes significant after the tenth cycle.

Computer Interface for an Electron Spectrometer

Responsible Personnel: R. Bastasz and V. C. Barton*

Brief Description: An interface has been developed to allow direct transfer of data from an electron spectrometer to a time-shared computer. The appropriate software has been implemented to store and display time-averaged photoelectron spectra. Possible future capabilities and applications of the computer interface include acquisition and analysis of Auger electron spectra, element depth profiles, and surface element maps.

Status: Small amounts of surface impurities can sometimes control the chemical behavior of a solid surface. In materials compatibility studies, this necessitates an accurate determination of the atomic composition and chemical properties of solid surfaces. X-ray photoelectron spectroscopy (XPS†) is a nondestructive technique well suited to these needs because it is able to identify the elements that compose a solid surface and measure the chemical oxidation state of surface atoms.

To detect submonolayer amounts of surface impurity atoms, the sensitivity of XPS must be measured through signal averaging. Signal averaging consists of recording and repeatedly summing photoelectron spectra until the signal/noise ratio of the summed spectra grows large enough to permit the detection of weak photoelectron signals. Several hours are usually required for a signal-averaged measurement.

Until now, the storage and display of signal-averaged photoelectron spectra obtained with the Compatibility Group's electron spectrometer have been in the form of analog recorder traces. This form of XPS data recording sacrifices some of the accuracy in the measurement because the data, being inherently digital in form, must be converted to an analog signal. In addition, the accuracy of the energy scale depends on the gain settings of the analog recorder and on the ability of the operator to align the ink pen on the graph paper. This loss of accuracy can be significant because changes

---

*Electronics Engineering Department, LLL.

†XPS and ESCA (electron spectroscopy for chemical analysis) are synonymous acronyms.

in the chemical environment of surface atoms are reflected in small shifts in the energies of the photoelectrons.

An interface has been designed and constructed between the electron spectrometer and a time-shared computer to allow direct transfer of the digital XPS data from the spectrometer to the computer. The interface consists of a serial data line from the Nicolet model 1074 signal averager of the spectrometer to a Data General Eclipse model C/300 computer. In addition, a control line has been installed between the computer and the interface to allow software control of data transmission. Connections have been made from the computer and the signal averager to a teletype near the spectrometer to enable the operator to monitor data transmission and to interact with the computer. Data are transmitted currently at a rate of 110 baud but modifications are being made to increase the transmission rate to at least 1200 baud. A diagram of the arrangement of the computer interface is given in Fig. 8.

Several Basic-language programs have been written to provide a convenient means of recording XPS data directly from the spectrometer onto a magnetic disk. Sample information and relevant instrument control parameters are stored, along with the digital spectral data. The stored data can be outputted in the form of photoelectron spectral line plots (Fig. 9). Although unsophisticated when compared with the graphics capabilities currently available elsewhere at LLL, these line plots provide an accurate measure of the photoelectron binding energies needed for materials compatibility studies.

With the digitized spectra now available, a variety of data analysis methods are possible including background subtraction, smoothing, resolution enhancement, and deconvolution of overlapping peaks. Also, the capability to calculate difference spectra to emphasize changes occurring in surface composition has been gained. This definitely will aid studies of adsorption, catalysis, and corrosion.

With the data link between the spectrometer and the computer now available, it becomes advantageous to automate other sections of the spectrometer. Two functions of the spectrometer that will benefit from automation are the multiplexing of Auger electron signals and the acquisition of scanning Auger microscopy (SAM) images. Entire Auger spectra can be acquired sequentially in digital form (during ion bombardment of a sample) and used to

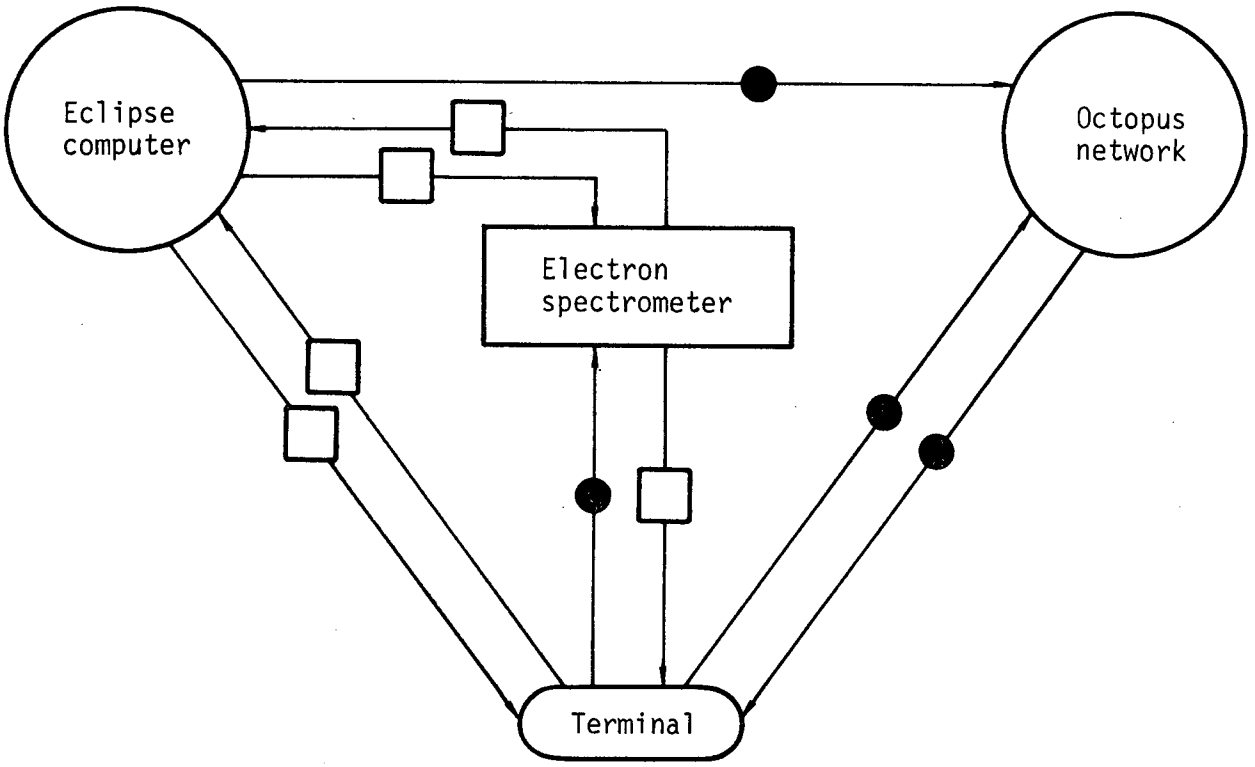

Fig. 8. Diagram of connections between the electron spectrometer and the computing facilities: □ = existing facility, ● = planned expansion.

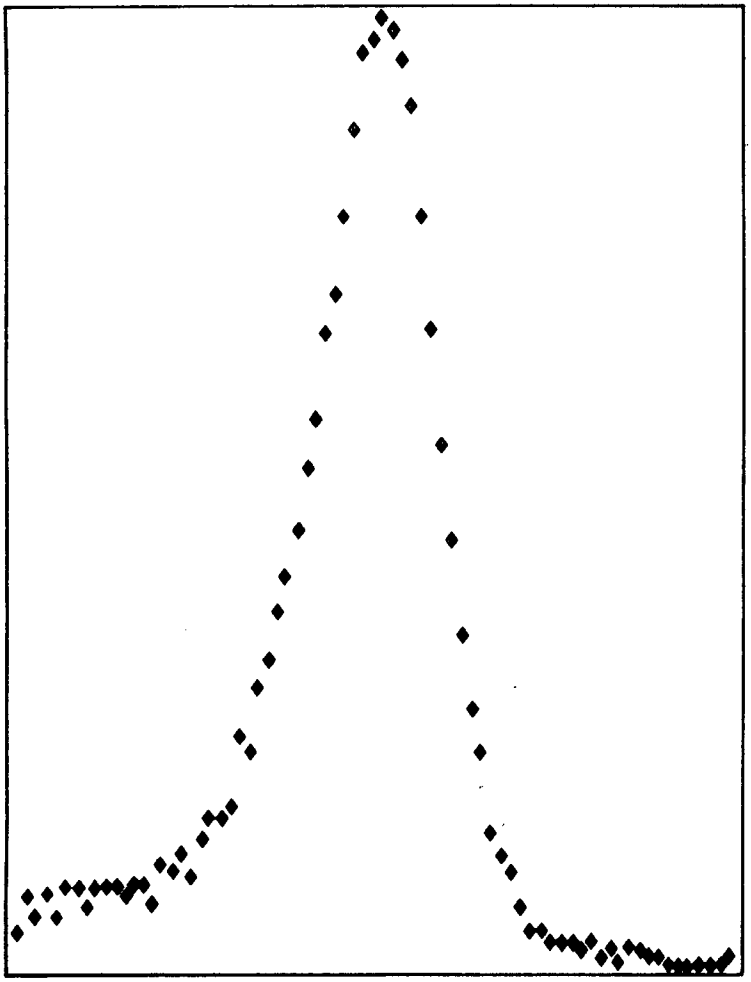

Fig. 9. Typical photoelectron spectrum line plot for the carbon 1s region; sixteen scans were made by pulse counting from 280 to 290 eV.

construct depth profiles of element abundance. Scaling problems associated with the current analog mode of operation will be eliminated when data is acquired in a digital form. It also will be possible to calculate and display element concentrations as a function of depth. Digital acquisition of element maps by SAM will allow the creation of surface element abundance contour plots. Such plots will identify concentration gradients on the sample surface. This capability will be especially useful in materials compatibility studies because the superposition of contour plots for different elements will point out locales of unusual chemical makeup.

We are planning to expand the computer-assisted electron spectrometer data system to permit better utilization of the instrument. An Octoport connection between the Eclipse computer and the Octopus network* is anticipated, along with a teletypewriter line and a TMDS monitor located at the spectrometer. This will allow time-shared access to the Octopus network so that the full resources of the computer center will be available for data analysis.

---

*LLL time-shared computer system.

Examination of Deposits on Exploding Gold Bridgewire Detonators

Responsible Personnel: J. W. Fischer, D. D. McCoy, and R. G. Meisenheimer

Brief Description: Exploding gold bridgewire detonators have been examined by optical microscopy, scanning electron microscopy, and electron microprobe spectrometry to characterize and identify anomalous deposits on the unexploded detonators.

Status: A series of exploding gold bridgewire detonators has been examined to document the presence and to identify the composition of extraneous material reported to exist on the unexploded detonators. Initial observations by optical microscopy revealed dark colored deposits on the solder-mount/plastic-base interfaces of several of the samples. The entire series of bridgewires was then systematically examined by optical microscopy to select appropriate candidates for further study. A detonator (MC 1693-1, Lot 102, S/N 9653) displayed two rather prominent anomalies of the type in question and was selected for further analysis to characterize and identify the composition of these deposits.

This detonator was subjected to a more extensive examination by optical microscopy; the presence of the deposits was documented visually by photomicroscopy. Figure 10 shows photomicrographs of the sample with the deposits identified by the arrows. The detonator was also examined with the scanning electron microscope to further define the morphological properties of these deposits. Figure 11 presents scanning electron photomicrographs of the deposits shown optically in Fig. 10.

Having physically characterized the deposits on detonator S/N 9653 by microscopic techniques, the sample was then examined in the electron microprobe to determine the elemental composition of the deposits. Figure 12 is an electron microprobe (EMP) target-current image of the solder mound previously shown in Figs. 10 and 11. The deposits are not directly visible in Fig. 12 but their locations are defined by the depressions in the image of the solder mound (identified by arrows). Figure 13 presents EMP copper Kα and sulfur Kα x-ray images, respectively, of the same region shown in Fig. 12.

The images in Fig. 13 indicate that the deposits in question are composed primarily of copper and sulfur; no other elements were detected in any significant concentration in the deposit formations. In addition, the

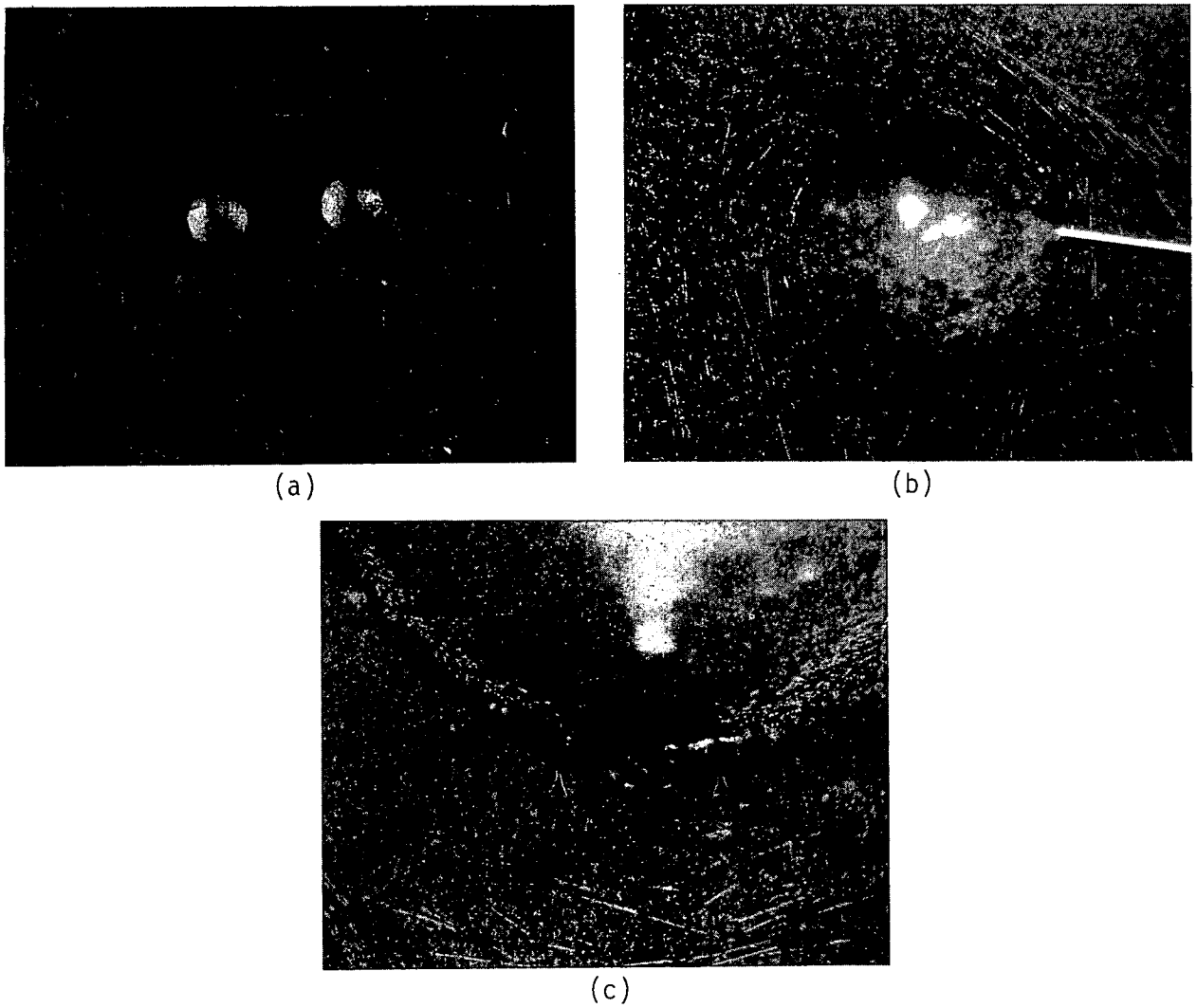

Fig. 10. Photomicrograph of detonator S/N 9653 (A-152-5) at magnifications of 14X (a), 63X (b), and 180X (c).

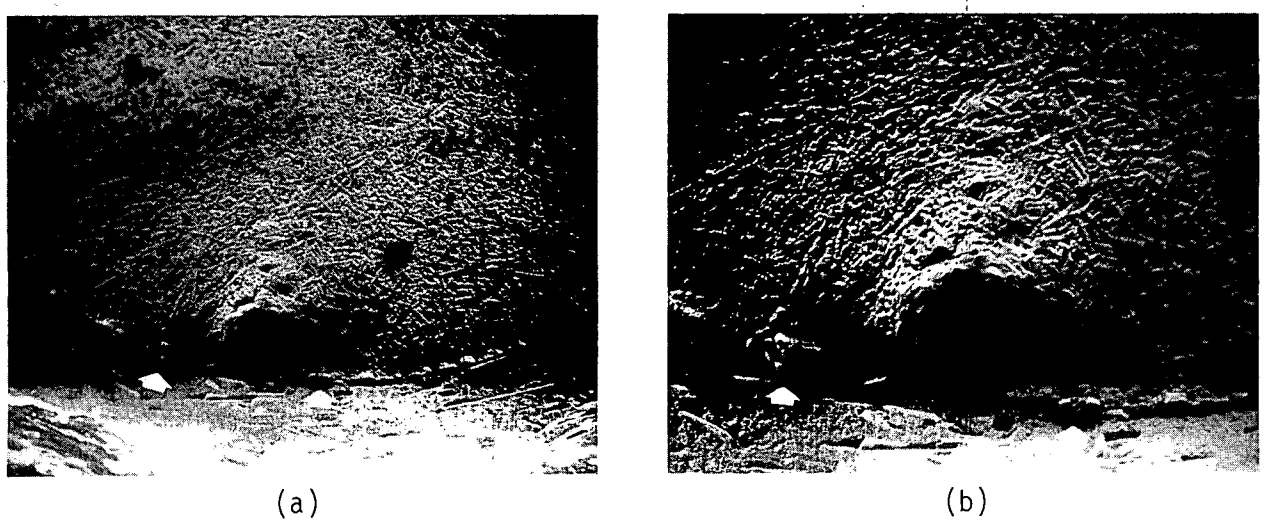

Fig. 11. Scanning electron photomicrographs of detonator S/N 9653 (A-152-44-24) at magnifications of 150X (a) and 500X (b).

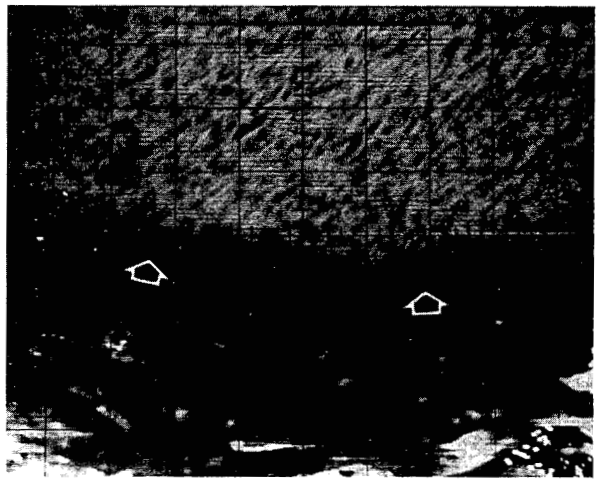

Fig. 12. EMP target current image of detonator S/N 9653 (A-152, EM265-14) at a magnification of 200X.

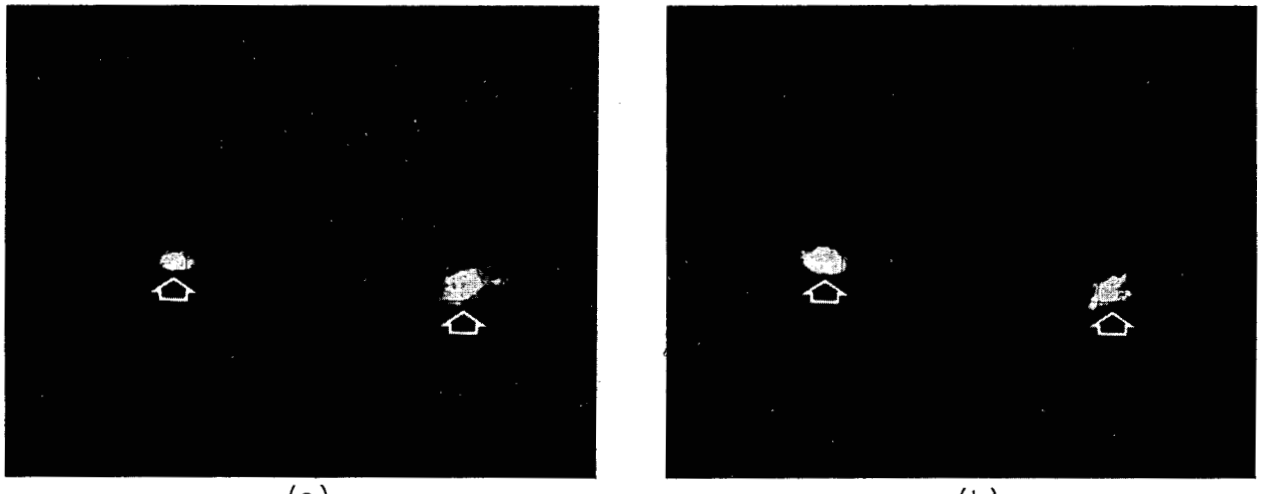

(a) (b)

Fig. 13. EMP copper (a) and sulfer (b) Kα x-ray images of detonator S/N 9653 (A-152, EM265-11 and EM265-10) at a magnification of 200X.

analysis revealed that the copper and sulfur in the deposits are present in approximately equal atom concentrations.

A second bridgewire detonator (MC 1693-1 Lot 102, S/N 9645) was chosen for examination. This detonator also had microscopically visible deposits in various regions of the solder-mount/plastic-base interface. It was analyzed in the electron microprobe to establish the composition of the deposit. An EMP target current image of a deposit-containing region of this detonator is shown in Fig. 14. The image of the gold wire is clearly visible in the upper left corner of the photograph. Figure 15 gives EMP copper Kα and sulfur Kα x-ray images, respectively, of the same region shown in Fig. 14. The x-ray image in Fig. 15b is not as extensive as that in Fig. 15a because of differences in instrument sensitivity for the elements in question; this does not indicate any real difference in relative elemental distribution. No other elements of significant concentration were found in these formations. The copper and sulfur again were found to be present in the deposit in approximately equal atom concentrations.

Thus, it appears that the dark colored deposits observed at the base of the solder mounds of various exploding gold bridgewire detonators are composed of copper and sulfur in approximately equal atom concentrations, suggesting the presence of a copper sulfide.

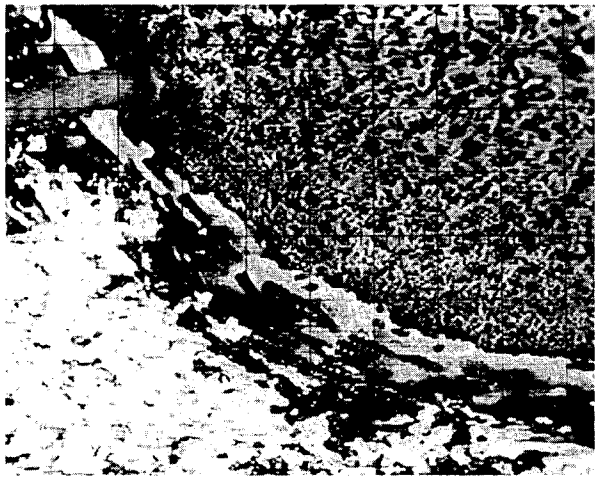

Fig. 14. EMP target current image of detonator S/N 9645 (A-152, EM-265-16) at a magnification of 200X.

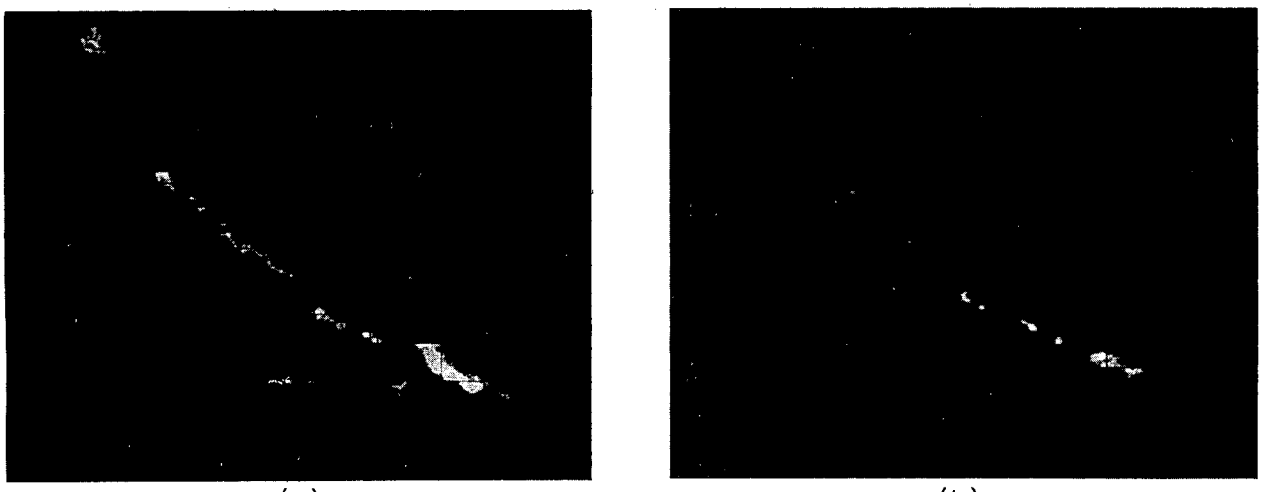

(a) (b)

Fig. 15. EMP copper (a) and sulfur (b) Kα x-ray images of detonator S/N 9645 (A-152, EM265-18 and EM265-17) at a magnification of 200X.

Carbon-13-NMR Study of Toluene-2,4-diisocyanate Polymers

Responsible Personnel: J. A. Happe, H. G. Hammon,* and C. M. Walkup

Brief Description: The nature of polymers formed by reacting toluene-2,4-diisocyanate with a polyalcohol is being studied by ^{13}C-NMR (nuclear magnetic resonance). The NMR spectra of several model systems have been obtained. With the aid of these models the ^{13}C-NMR spectrum of an actual reaction mixtures has been interpreted.

Status: Toluene diisocyanate (TDI) has two reactive isocyanate groups. At room temperature, the para-isocyanate is most reactive toward an alcohol. At higher temperatures, the ortho- and para-isocyanate groups tend to become equally reactive. Information about the course of the reaction under various conditions is needed in the preparation of polymers with specific properties. For this reason, ^{13}C-NMR has been used to examine both reactants and reaction products. One of our primary interests has been the determination of the relative numbers of TDI molecules which have undergone reactions at the ortho position, the para position, or at both the ortho and para positions to form a final product. Unreacted TDI also may be found in such a reaction product.

The TDI molecule has six aromatic carbon atoms, two isocyanate carbons, and a methyl carbon. The ^{13}C-NMR spectrum is shown in Fig. 16a. The methyl carbon resonance occurs in a different region of the spectrum and is not shown. Separate peaks are found for each of the aromatic carbons, assigned as shown. The two isocyanate resonances are indistinguishable from each other.

When two moles of TDI react with one mole of a polyalcohol containing two OH groups per molecule, the reaction at room temperature should produce, primarily, para-reacted aromatic groups in a product resembling the following:

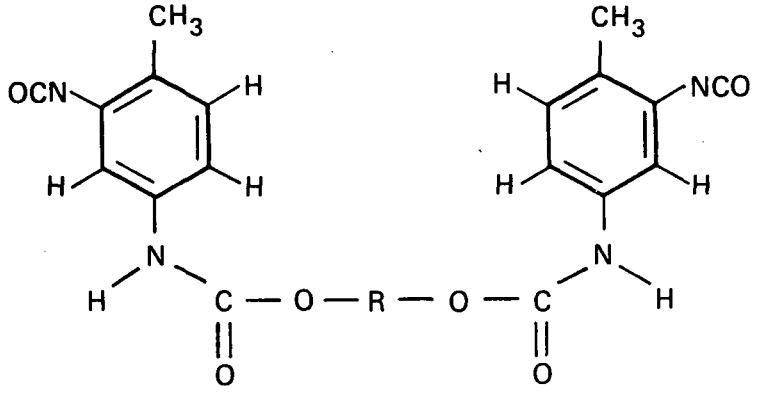

*Organic Materials Division, LLL.

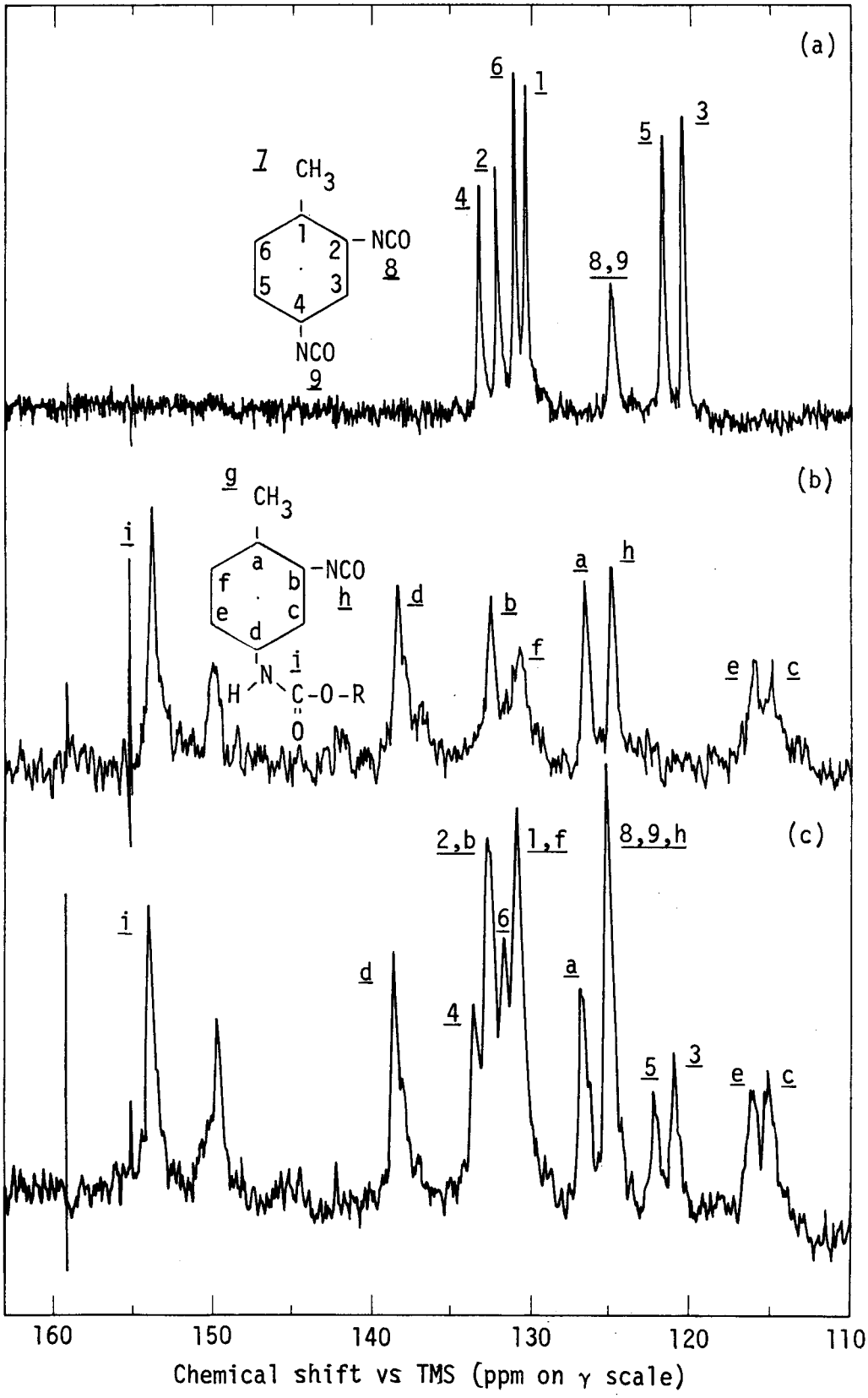

Fig. 16. Fourier transform ^{13}C-NMR spectra taken at 15.077 MHz and covering the phenyl region: (a) 2,4 toluene diisocyanate (TDI), (b) product of the reaction of TDI and a dialcohol in a mole ratio of 2:1, and (c) product of the reaction of TDI and a dialcohol in a mole ratio of 3.25:1.

The ^{13}C-NMR spectrum from such a product is shown in Fig. 16b. Again, separate peaks are found for the various chemically different carbon atoms of the molecule. Reaction at the para-isocyanate group shifts the various resonances from their positions in the TDI molecule. The shifts are such that a number of product resonances are well separated from the original TDI peaks. This enables us to distinguish unreacted TDI from para-reacted material. Figure 16c shows the ^{13}C-NMR spectrum of a product containing excess TDI. The spectrum is clearly the superposition of TDI and para-reacted TDI resonances.

To determine whether there are product molecules where reaction has occurred at both ortho- and para-isocyanate positions, a model compound with the following structure was prepared from TDI and ethylalcohol:

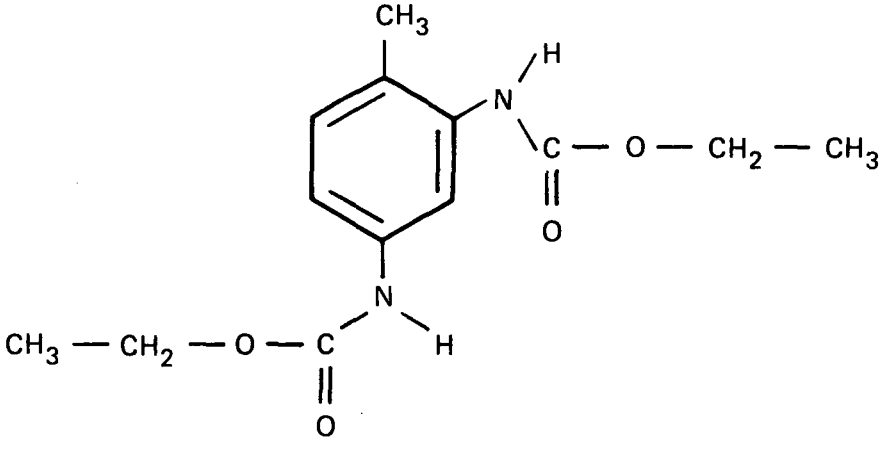

The ^{13}C-NMR spectrum of this material reveals that the meta-carbon atom resonance (resonance between the two reacted isocyanate groups) occurs at a field strength higher than that for a monoreacted ring system. Its chemical shift of 112.49 ppm should allow its detection and measurement in products which also contain TDI, ortho-reacted or para-reacted TDI molecules.

From an examination of the ^{13}C-NMR shifts observed thus far, a tentative prediction of a 117.9-ppm shift can be made for the C5 carbon atom of ortho-reacted TDI. It appears that it will be possible to determine the amount of ortho-reacted product from the intensity of a ^{13}C-NMR peak anticipated at this field strength. In spectra taken so far, ortho reaction alone has not been observed.

Estimation of the Solubility of TATB in Various Solvents

Responsible Personnel: W. Selig

Brief Description: A method for estimating the solubility of TATB* in various solvents was developed using spectrophotometry. As a result of this study, we consider it unlikely that a solvent will be found in which TATB is soluble to an extent greater than 0.1% (w/v). Exceptions are the "superacids" in which TATB is soluble to greater than 10%.

Status: We previously reported the solubility of the explosive material TATB in various sulfuric acid:water mixtures.† Since then, we have found several other so-called "superacids" in which TATB has a solubility similar to that in concentrated sulfuric acid. These acids are chlorosulfonic acid, fluorosulfonic acid, and trifluoro-methanesulfonic acid. We must stress that these acids are highly corrosive and hygroscopic, reacting violently with water and thus are difficult to handle.

Of the more conventional solvents, we have found none in which the solubility of TATB exceeds 0.08% (w/v). In fact, we do not believe that any significantly better solvents for TATB will be found. The "best" of this series of solvents with the approximate solubilities of TATB are listed in Table 2.

Table 2. Solubility of TATB in the "best" solvents.

Solvent	Solubility, ppm
Methanesulfonic acid	820
Hexamethylphosphortriamide	150
Ethanesulfonic acid	120
Dimethylsulfoxide	70
Hexafluoroacetone sesquihydrate	68
N-methyl-2-pyrrolidinone	58
N, N-dimethylacetamide	31

*1,3,5-Triamino-2,4,6-trinitrobenzene.

†See Ref. 9, p. 24.

Our method of estimating the solubility is simple. A small, known amount of TATB is placed in a volumetric flask (25 or 10 cm^3). The solvent to be examined is added and the flask is placed in an ultrasonic bath for several minutes at an ambient temperature not to exceed 30°C. The flask is then taken out of the bath and left at room temperature until either the solid TATB has settled out or for a minimum of two days. The spectrum of the solution in a 1-cm cell is then taken in the near UV region, from about 400 to 260 nm, and compared to a solvent blank. Dilutions are made as required. The approximate solubility of TATB (in parts per million) is calculated from the formula:

TATB solubility = (Absorbance) (10.33) (dilution factor).

Where no dilution is required, the dilution factor obviously is unity.

This method is based on the following assumptions:

- The molar absorbance of TATB in any solvent approximates that in concentrated sulfuric acid; i.e., approximately 25,000 at 324 nm.[12]
- The density of the solvent is reasonably close to unity.
- The solution measured is saturated.

The calculation is based on the relationship,

$$\varepsilon = A/C ,$$

where ε is the molar absorbance (~25,000), A is the absorbance measured, and C is the concentration ($mol \cdot dm^{-3}$). The concentration of a saturated solution therefore equals the measured absorbance divided by 25,000. The concentration (milligrams per cubic decimeter or parts per million) equals absorbance times 10.33. Further details of this work are presented in Ref. 13.

---

12. H. E. Ungnade, 1,3,5-triamino-2,4,6-trinitrobenzene (TATB) — Preparation and Purification, Los Alamos Scientific Laboratory, Rept. GMX-2-R-64-1 (1963), pp. 10-11.

13. W. Selig, Estimation of the Solubility of 1,3,5-Triamino-2,4,6-Trinitrobenzene (TATB), Lawrence Livermore Laboratory, Rept. UCID-17412 (1977).

Determination of Primary, Secondary, and Tertiary Amines

Responsible Personnel: W. Selig and G. L. Crossman

Brief Description: A primary amine, 1,6-hexanediamine, and a secondary amine, 1,3-dipiperidylpropane, were analyzed separately and in mixtures by different methods. Our results show that the salicylaldehyde method for secondary and tertiary amines[14] must be verified for each amine mixture to be analyzed.

Status: We have reported previously a modification of the salicylaldehyde method for the analysis of secondary and tertiary amines in the presence of primary amines.[15] For the titration of total amine, we used 0.1 N perchloric acid in glacial acetic acid. For secondary and tertiary amines, we used 0.1 N hydrochloric acid in ethylene glycol/isopropanol. This method proved satisfactory for mixtures of n-butylamine and di-N-butylamine.

This quarter, additional work was done with 1,6-hexanediamine, a primary amine, and with 1,3-dipiperidylpropane, a secondary amine. In addition to the titrants mentioned above, we also used 0.5 N hydrochloric acid in 2-propanol/methyl cellosolve, as recommended by the Jefferson Chemical Company.

For the determination of total amine, titration with 0.1 N perchloric acid/acetic acid yields unambiguous results. Glacial acetic acid serves as a "leveling" solvent and makes all bases appear to be the same strength. The titrant used by the Jefferson Chemical Company yields two breaks for 1,6-hexanediamine. This indicates the presence of an impurity of different basic strength than 1,6-hexanediamine.

The Jefferson Chemical Company solvent system yielded better titration curves for the salicylaldehyde method than did our solvent system. However, further work should be done with the Jefferson titrant, modified to 0.1 N HCl in 2-propanol/methyl cellosolve so that titrants of the same normality can be compared.

---

14. S. Siggia, J. G. Hanna, and I. R. Kervenski, Anal. Chem. 22, 1295 (1950).
15. General Chemistry Division Quarterly Report, January through March 1974, Lawrence Livermore Laboratory, Rept. UCID-15644-74-1 (1974), p. 2.

We were surprised to find that 1,6-hexanediamine yielded a titration curve after reaction with salicylaldehyde. Obviously, the Schiff base that is formed in the reaction of the primary amine with salicylaldehyde is sufficiently basic to be titratable. Both salicylaldehyde methods yielded recoveries of only 93.5% for the secondary amine, based on the previously determined purity of this amine. Hence, even for strongly basic amines, the results are only approximate.

We must point out that very little has been published on titrimetric methods for secondary and tertiary amines since the original paper in 1950.[14] Thus, each amine mixture submitted for analysis must be carefully examined; difficulties can be expected, especially with complex mixtures.

Ion-Selective Electrode Technology

Responsible Personnel: W. Selig

Brief Description: An electrode sensitive to hydrogen sulfide gas and a sulfate-ion-specific electrode were examined. These electrodes were expected to function as logarithmic sensors, enabling the determination of H_2S and SO_4^{2-} species. However, neither was found to yield satisfactory results.

Status: Lazaar Research Laboratories markets a hydrogen-sulfide-gas-sensing electrode that was of interest to us for measurements in the geothermal effort. This sensor was expected to indicate the concentrations of hydrogen sulfide in solutions after acidification over the range of 1 to 100 ppm. Several attempts to calibrate this electrode using acidified, standard sodium sulfide solutions have failed. The electrode yielded erratic responses in each case. Moreover, we consider its construction awkward; it is somewhat difficult to assemble the electrode before taking measurements.

Chemtrix Incorporated markets a sulfate-ion-selective electrode which was also of interest for the geothermal project. This sensor, in combination with a reference electrode, was expected to measure the sulfate ion over the range of 10 to 10,000 ppm at pH 5. However, we examined two of these sulfate sensors and were not able to obtain satisfactory calibration curves.

Investigation of Discrepancies between Chromatographic and Mass Spectrometric Data

Responsible Personnel: J. C. Newton and J. E. Clarkson

Brief Description: Discrepancies between data produced by gas chromatographic and mass spectrometric analyses have been found. To resolve these differences, we have analyzed several vendor "certified" standards. Our results show that "certified" gas mixtures are supplied with erroneous analyses.

Status: Differences in the gas composition determined by mass spectrometry and gas chromatography have been observed in samples from various programs. The causes for these discrepancies have been investigated. They are explained very satisfactorily in terms of errors in the composition of the standard gas mixtures which are used to calibrate the chromatographic instrumentation.

The values given by the vendor previously have been accepted without question for each standard gas mixture because they are "certified" to be within ±2% of the component value stated. To verify the composition of the standards, we analyzed these gas mixtures with the CEC 21-103C mass spectrometer. Significant differences were discovered. Table 3 lists typical results obtained for three "certified" standards. The relative percent difference exceeds 2% for some components. Table 4 shows similar results for a mixture of seven organic compounds.

We are continuing to investigate these deviations; however, we believe that many of the "certified" gas standards have not contained the mixture as stated on the label. Confirming evidence for this was found by purchasing and analyzing two "primary" gas standards. These standards are made by weight and are guaranteed to be accurate to ±1% of the component value reported. One of these standards was used to calibrate the gas chromatograph. Then, we analyzed a "certified" standard. The results for the "certified" standard agreed very favorably with the LLL mass spectrometric data but not with the analysis provided by the vendor.

In the future, all standards used for gas chromagraphic analysis will be checked first by mass spectrometry.

Table 3. Comparison of vendor analyses and LLL mass spectrometric results for gas chromatographic gas standards.

Component	Vendor, Vol%	LLL, vol%	Difference, vol%	Relative difference, %
Tank 52830				
N_2	52.85	56.67	+3.82	6.74
O_2	0.98	0.94	-0.04	-4.26
Ar	1.10	0.94	-0.16	-17.02
CO_2	9.35	9.52	0.17	1.79
CO	9.33	9.28	-0.05	-0.54
H_2	3.57	3.57	0.00	0.00
CH_4	22.82	19.09	-3.73	-19.54
Tank 16045				
N_2	53.36	50.92	-2.44	-4.79
O_2	1.51	1.45	-0.06	-4.14
Ar	35.36	37.82	2.46	6.50
CO_2	—	0.05	—	—
CO	4.36	3.96	-0.40	-10.10
H_2	1.05	1.16	0.11	9.48
CH_4	4.36	4.64	0.28	6.03
Tank 40299T				
N_2	21.70	21.90	0.20	0.91
O_2	—	—	—	—
Ar	—	—	—	—
CO_2	20.26	20.49	0.23	1.12
CO	20.60	20.56	-0.04	-0.19
H_2	18.34	18.01	-0.33	-1.83
CH_4	19.10	19.05	-0.05	-0.26

Table 4. Comparison of vendor analyses and LLL mass spectrometric results for gas chromatographic gas standards.

Component	Vendor, vol%	LLL, vol%	Difference, vol%	Relative difference, %
CH_4	12.22	12.3	-0.08	-0.65
C_2H_4	1.13	1.19	-0.06	-5.04
C_2H_6	1.06	1.10	-0.04	-3.64
C_3H_6	1.51	1.93	-0.42	-21.76
C_3H_8	1.58	1.68	-0.10	-5.95
$i\text{-}C_4H_{10}$	0.87	1.12	-0.25	-22.32
$n\text{-}C_4H_{10}$	0.80	1.02	-0.22	-21.57

Analytical Research and Development for the Energy Programs

Automated, Portable, On-Line Mass Spectrometer for the Oil Shale Program

Responsible Personnel: R. W. Crawford, C. J. Morris, K. Ernst, H. R. Brand, C. L. Pomernacki,* J. R. Elliot,* and M. L. Malachosky†

Brief Description: Several types of oil shale experiments require rapid gas analyses to develop kinetic data and to measure the effects of changes in the supply gas composition. A commercial quadrupole mass spectrometer is being modified and computer-automated to provide this information. It will be designed for on-line operation and portability among several experiments.

Status: Initial experiments with an existing instrument indicated that a properly designed quadrupole mass spectrometer could perform the required gas analyses. The major problems involved sampling and cracking-pattern stability. It appears that these problems can be minimized with the new instrument.

The inlet of the instrument is designed to sample a flowing gas stream at atmospheric pressure with an initial pressure drop across an 86-cm-long heated capillary tube. The pressure at the end of this tube is held at approximately 67 Pa (0.5 Torr) by a mechanical pump. A gold foil with two 0.076-mm (3-mil) holes is used as a molecular leak to introduce gas into the quadrupole analyzer from the low-pressure end of the capillary. The combination of a viscous and molecular leak is necessary to obtain quantitative results over a broad concentration range. In addition, the inlet is provided with interlocks to protect the spectrometer in case of pump or electrical failure.

The calibration system consists of nine high-pressure cylinders of gas that are connected to a common manifold. Six of these are the pure gases: CO, CO_2, H_2, CH_4, C_2H_6, and Ar. The other three are mixtures of the above

---

*Electronics Engineering Department, LLL

†Mechanical Engineering Department, LLL.

gases, and in two cases, contain higher hydrocarbons. An extra port is available for occasional calibration with C_3 and C_4 hydrocarbons.

Instrument sweeping and data logging are performed by a computer. Present implementation is designed for either a PDP-8 series or a D-112 computer; plans for a future LSI-11 system also are being made. The computer will be remote from the spectrometer and the interface has been designed and tested to work with 300 m (1000 ft) of interconnecting cable. One twisted pair controls the rf sweep and therefore the mass sweep of the spectrometer. A 16-bit D/A converter gives excellent resolution (1 part in 66K). A 1-MHz V/F converter sends the peak-height signal to the computer over a second twisted pair. The useful dynamic range of this measurement is one part in 32K. The hardware for this system has been completed and is functioning well.

Software development is almost complete. When fully developed, the following functions will be available:

- Calibrating the mass scale.
- Recording the cracking pattern and sensitivity coefficients for standards.
- Recording spectra of the unknown with predetermined timing between runs.
- Calculating the amounts of the various species in the unknown mixture and outputting the analysis results to a teletypewriter.

Preliminary tests have been made to determine quantitative performance of this mass spectrometer. The instrument was first tested with a calibrated gas mixture using two flowmeters — one connected to argon and the other to CO_2. Mixtures of these gases, ranging from 5 to 95% of each component, were introduced and determined on the basis of the sensitivity of each pure gas. The results were obtained within the accuracy of the flowmeter calibrations (~2%).

We also checked the cracking pattern and absolute sensitivity of the instrument for stability by analyzing air every 15 min overnight. Figure 17 shows plots of the intensities of the major peaks in air. This stability is satisfactory because the ratios of the various peaks are the critical parameters, not the total intensity. Figure 18 illustrates the stability of the ratios with plots of the cracking pattern of N_2 (14/28), O_2 (16/32), and argon (20/40) in air. The mass-20/mass-40 ratio is noisy because the mass-20

peak for air is very low in intensity (barely above the threshold). These results do indicate that the stability of the cracking pattern is very good.

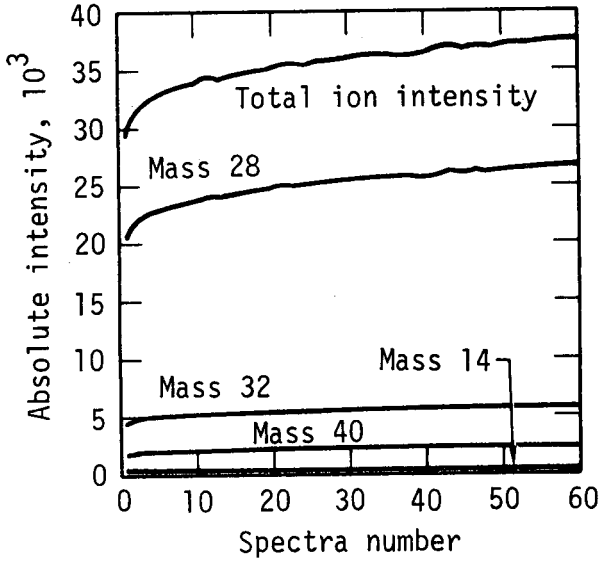

Fig. 17. Stability of mass-peak intensities during repeated analyses of air. Mass spectra were obtained at 15-min intervals.

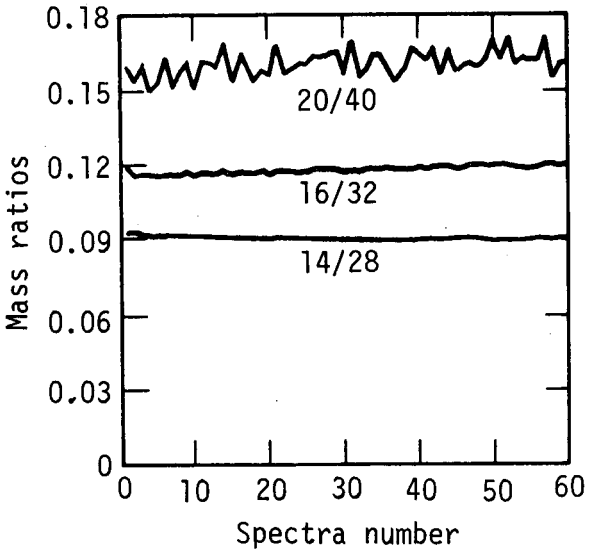

Fig. 18. Stability of mass-peak intensity ratios during repeated analyses of air. Mass spectra were obtained at 15-min intervals.

Determination of Carbonate Minerals in Oil Shales

Responsible Personnel: R. Lim, L. J. Gregory, K. L. Leach, and S. Deutscher

Brief Description: We have continued our attempts to resolve the discrepancies between our results and those reported by Young, Smith, and Robb[16] for the Colorado Green River oil shale.

Status: Previous work at LLL[17] revealed discrepancies between our results and those of U.S. Bureau of Mines workers[16] for the cation values of the Green River oil shales. Discrepancies also exist between the carbon dioxide content calculated from the cation values and that determined by acid evolution. The procedures employed involve selective leaching of the oil shale and extraction of the cations, followed by determination of the cations by atomic absorption spectrophotometry and of the carbonates by acid-evolution of CO_2. From this information, the mineral composition of the oil shale can be inferred.

To further investigate the discrepancies, we checked our calcium determination method to see if it was faulty. We extracted a series of Green River oil shales by successively leaching each sample with water and acid. In the acid treatment, the sample was leached with approximately 75 cm^3 of 6 N HCl, heated to 90°C and stirred constantly for 15 min.

Calcium in aliquots of the acid filtrate then was determined by three different methods:

- Atomic absorption spectrophotometry with the addition of lanthanum to make a 0.5% lanthanum solution.[18] (This is the method used by the USBM laboratory.)
- Atomic absorption spectrophotometry with a nitrous oxide-acetylene flame.[18]

16. N. B. Young, J. W. Smith, and W. A. Robb, Determination of Carbonate Minerals of Green River Formation Oil Shales, Piceance Creek Basin, Colorado, U.S. Bureau of Mines, Rept. 8008 (1975).
17. General Chemistry Division Quarterly Report, September through December 1976, Lawrence Livermore Laboratory, Rept. UCID-15644-76-4 (1977), p. 48.
18. Analytical Methods for Atomic Absorption Spectrophotometry, Perkin-Elmer Corporation (September 1976).

- Double precipitation of calcium oxalate, followed by ignition to calcium carbonate and weighing.[19]

The results of analyses by these methods are given in Table 5. The atomic absorption method with the addition of lanthanum as a chemical releasing agent agrees well with the gravimetric determination as the oxalate. The atomic absorption method using a nitrous oxide-acetylene flame yielded lower results. Apparently, the temperature of the nitrous oxide flame is not high enough to decompose some of the compounds in the oil-shale acid-extraction solutions. However, added lanthanum is an effective releasing agent, as shown by the excellent agreement of results with the gravimetric method.

To find out what various extraction steps of the procedure were leaching, the water soluble portions were examined for calcium and magnesium. If calcium and magnesium are dissolved in sufficient concentration to introduce an error, this might explain why samples No. 7, 48, 76, and 77 had higher CO_2 results from the acid evolution of the water soluble portions. Small amounts of dolomite could be dissolving into the water leach; the Handbook of Chemistry and Physics lists a solubility for dolomite of 32 mg per 100 cm^3 of water at 18°C.

We found that small but significant amounts of calcium and magnesium were extracted by water. Thus, small amounts of dolomite are probably dissolved by the water leach. For two of the samples, the calcium and magnesium concentrations in the water-soluble portion were as high or higher than the concentrations of sodium dissolved from nahcolite.

From these findings, we have concluded that the extraction procedure is not very accurate and can only be treated as a good estimate of the carbonate minerals present. Our calcium results still show a positive bias compared to those reported by Young, Smith, and Robb. However, we feel they are accurate because of the excellent agreement obtained with the gravimetric method. The complete details of this work are presented in an LLL report now in preparation.

---

19. I. M. Kolthoff and E. B. Sandell, Textbook of Quantitative Inorganic Analysis (MacMillan Co., New York, 1952) 3rd ed., pp. 337-351.

Table 5. Determination of calcium in 6 N HCl extracts of Green River oil shale.

Sample No.	Calcium, wt%		
	A.A.S. with La additions	A.A.S. with a nitrous oxide-acetylene flame	Double precipitation of calcium oxalate
7-1	5.67	4.11	5.80
7-2	5.74	4.12	5.81
39-1	2.79	1.74	2.95
39-2	2.87	1.76	2.96
48-1	5.91	4.45	5.96
48-2	5.86	4.38	5.95
55-1	5.64	4.10	5.68
55-2	5.58	4.04	5.68
56-1	4.61	3.41	4.76
56-2	4.70	3.41	4.78
76-1	3.09	2.24	3.16
76-2	3.01	2.20	3.18
77-1	6.67	5.04	6.69
77-2	6.65	5.00	6.66

Continuous Determination of Hydrogen Sulfide at the San Diego Gas & Electric Company Geothermal Plant

Responsible Personnel: C. J. Morris

Brief Description: We have developed a method to provide continuous determinations of gaseous H_2S at the San Diego Gas & Electric (SDG&E) Co. geothermal plant at Niland, California. The facility was monitored for seven days and calculations were made estimating the quantity of H_2S emitted into the atmosphere.

Status: Environmental standards require the monitoring of the amount of H_2S introduced into the atmosphere during operation of the SDG&E Co. geothermal-loop experimental facility. The monitor chosen for this series of analyses was an Ecolyzer Model 2407 H_2S analyzer. This instrument is capable of H_2S analysis at the 0- to 5000-ppm level and was selected on the basis of our previous use of a similar, lower-level (0- to 50-ppm) analyzer.

A series of continuous gas sampling tests, 4 h in duration, with the Ecolyzer was run at the stack of the SDG&E Co. facility. The results demonstrated that, at H_2S levels of 1500 to 3000 ppm, there was a steady downward drift of the indicated level of H_2S, up to 20% from the true value. Probably, this was caused by a slow rise in the temperature of the cell (due to the warm gas sample) or to gradual cell saturation. Although some cooling of the gas stream is necessary to prevent water from plugging the instrument, reducing the stack sample to ambient temperature was not desirable because losses of H_2S by absorption are possible. Therefore, we tried to "regenerate" the cell by running ambient air through the cell between the periods of stack sampling. This procedure worked very well and also allowed us to check the instrument for zero shift.

The instrument was calibrated frequently (every 4 h) during these tests to check for long-term drift. The results demonstrated periods of stability ranging from 8 to 48 h; calibration runs every 8 to 12 h therefore are required for optimum accuracy.

On the basis of these experiments, an H_2S monitoring system was built (see Fig. 19). Included in the weather-tight enclosure was the H_2S monitor, recorder, solenoid valving, and the adjustable valve timer. At present, the automatic time sequence is set for 5 min of stack sampling followed by

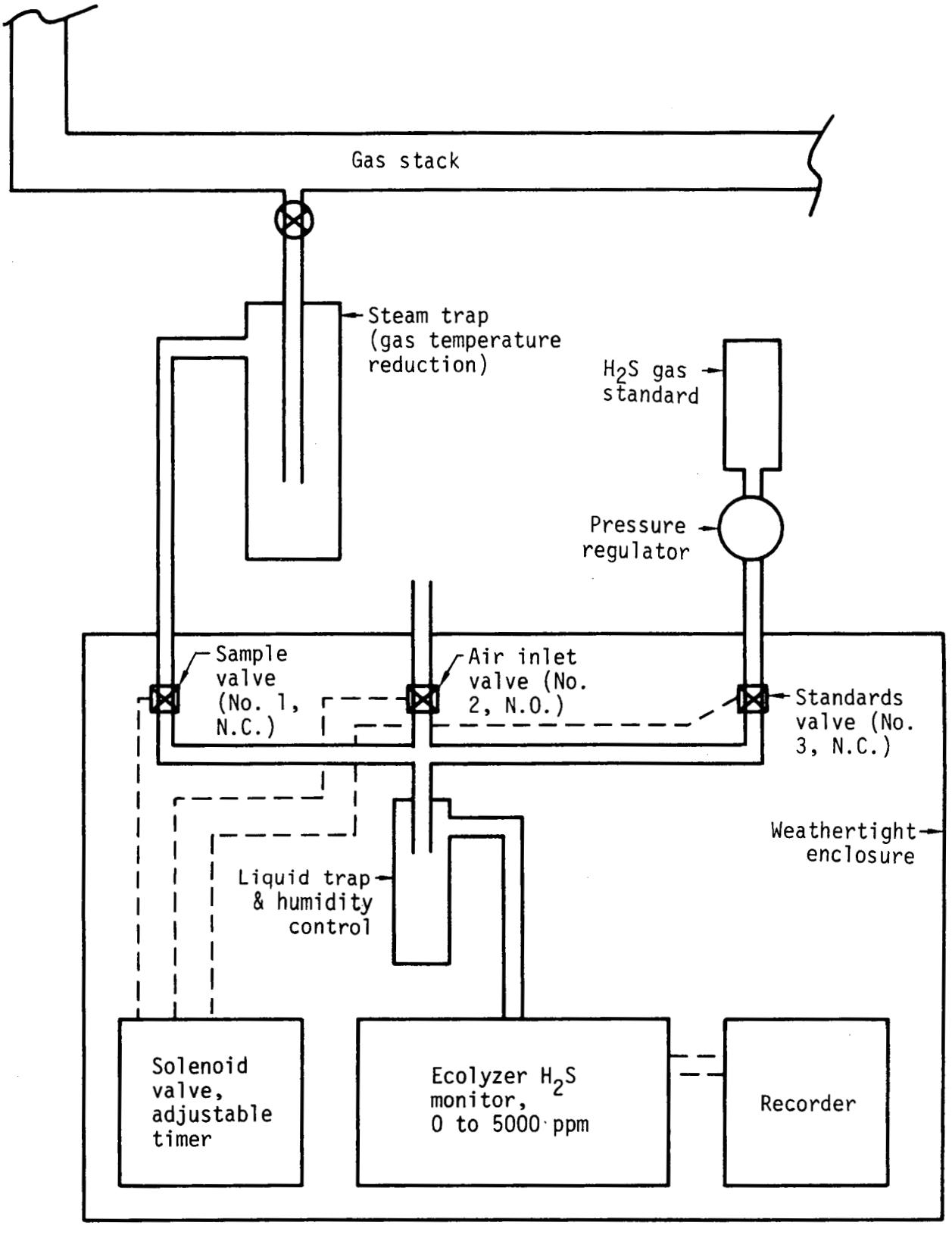

Fig. 19. Continuous gas monitor for H_2S.

10 min of ambient air. This cycle is repeated continually except for an interruption every 6 h to admit the calibration gas.

From January 6 to 12, 1977, the system was attached to the stack at the SDG&E Co. facility at Niland and the H_2S was monitored continuously. Figure 20 graphs the level of H_2S (by volume) vs time. The average value was computed to be 2410 ppm H_2S with concentrations ranging from 1580 to 2950 ppm. The approximate accuracy of the H_2S analysis is ±5%.

Table 6 lists the calculated estimates of the total H_2S released to the atmosphere, based on the above analysis and on the best available gas and brine flow parameters. However, at this time, the total gas flow is only an estimate because reliable plant instrumentation is not yet available.

Table 6. Estimation of emission rate of H_2S by the San Diego Gas & Electric Co. geothermal-loop experimental facility.

Average flow rate of brine through plant	400,000 lb/h
Steam flow rate (approximately 15% estimated quality)	60,000 lb/h
Total flow rate (total gas/steam ratio estimated to be about 0.015, total gas approximately 98% CO_2)	900 lb/h
Average H_2S concentration	2,410 ppm by volume
H_2S emitted to atmosphere	1.68 lb/h (760 g/h)

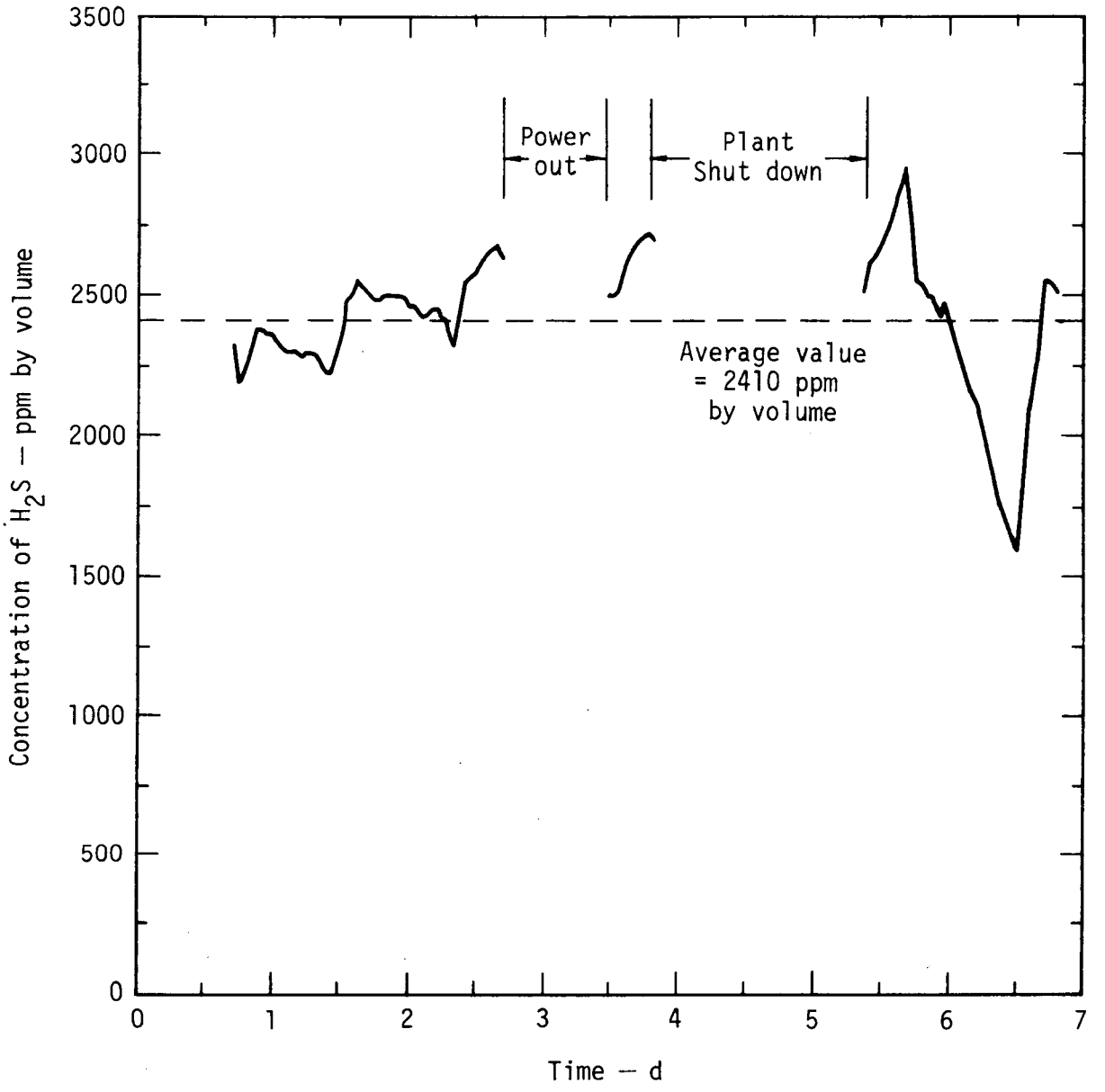

Fig. 20. Indicated levels of H_2S at exhaust stack of the San Diego Gas & Electric Co. facility. The plant was monitored from January 6, 1977 (Day 0) through January 13, 1977 (Day 7).

Geothermal Brine and Solids Characterization

Responsible Personnel: J. H. Hill, C. J. Morris, C. H. Otto, and R. W. Ryon

Brief Description: We are providing technical and analytical support for the Geothermal Total Flow and Industrial Support Programs. This work involves brine characterization, brine modification and scale control studies, suspended solids characterization and control, and effluent characterization.

Status: Previous work on the characterization and acidification of geothermal brine* indicated that equilibria involving CO_2 and NH_3 are primarily responsible for acid consumption in brine from Magmamax Well No. 1 as well as for changes in pH that occur when the brine is flashed. To quantify the effects of these CO_2-NH_3 equilibria, a series of samples was taken during operation of the LLL Total Flow Test Unit in April 1977.

Two sets of samples consisting of wellhead brine, separated brine, and separated steam were analyzed for total ammoniacal nitrogen (NH_3, NH_4^+, NH_4OH) by ion-selective electrode potentiometry. The results, expressed in parts per million of NH_3, are shown in Table 7.

Results for the two sets of steam samples taken by different techniques indicate that some gaseous NH_3 may have been swept through the sampler. The sampling apparatus is being redesigned to eliminate this problem. Because of this sampling problem, these data are not conclusive. However, our best estimate is that the whole brine contains ammoniacal nitrogen equivalent to approximately 400 ppm NH_3. Also, the ammoniacal nitrogen is distributed approximately evenly between the separated brine and the separated steam.

Acid consumption was measured by titrating samples of separated and wellhead brine (see Fig. 21). The addition of 105 ppm of HCl was required to acidify the separated brine to pH 3.5. The total CO_2 (CO_2, H_2CO_3, HCO_3^- and CO_3^{-2}) content of a separated brine sample taken concurrently in a pressure bottle was 162 ppm. This CO_2 content is equivalent to 130 ppm of HCl in the reaction of HCO_3^- with HCl. These data, together with the pH value (6.0) of the separated brine, indicate that HCO_3^- is the primary acid-consuming species in the separated brine.

---

*See Ref. 1, p. 39.

Table 7. Concentrations of total ammoniacal nitrogen in geothermal samples.

Sample Number	Temperature, °C	Pressure, psi	Sample Type	Concentration, ppm NH_3
LM-B1-7F90	195	250	Wellhead brine	391
LM-B1-TF90A[a]	195	250	Wellhead brine	410
LM-SB-TF91	195	250	Separated brine	408
LM-SS-TF92	195	250	Separated steam	357
LM-SS-TF92A[b]	195	250	Separated steam	394
LM-B1-TF98	180	235	Wellhead brine	366
LM-B1-TF98A[a]	180	235	Wellhead brine	374
LM-SB-TF99	178	235	Separated brine	387
LM-SB-TF99A[a]	178	235	Separated brine	366
LM-SS-TF100[a]	180	235	Separated steam	340
LM-SS-TF100A[b]	180	235	Separated steam	418
LM-E3-TF101	—	—	Elbow, Station No. 3	453
LM-AR-TF102	—	—	Atmospheric receiver	476

[a]Sample bottle contained approximately 5 cm^3 dilute HCl.
[b]Sample collected by bubbling into 250 cm^3 dilute HCl.

Assuming a steam quality of 10%, the acid consumption of the whole brine can be calculated from the acid consumption of the separated brine and the NH_3 content of the separated steam.

- Quantity of HCl required to acidify 900 g of separated brine to pH 3.5:

$$900 \text{ g brine} \times \frac{105 \text{ mg HCl}}{1000 \text{ g brine}} = 95 \text{ mg HCl} .$$

- Quantity of HCl required to react with NH3 in 100 g of separated steam:

$$100 \text{ g steam} \times \frac{400 \text{ mg } NH_3}{1000 \text{ g steam}} \times \frac{36.5 \text{ mg HCl}}{17.0 \text{ mg } NH_3} = 86 \text{ mg HCl} .$$

Therefore, a total quantity of 181 mg of HCl is required to react with 1000 g of whole brine. Thus, 181 ppm of HCl should be required to acidify a sample of whole brine to pH 3.5. The titration curve for the wellhead sample (Fig. 21) indicates that 140 mg of HCl were required to acidify the sample to pH 3.5. This value is in good agreement with the calculated value, considering the error known to occur when sampling the two-phase flow.

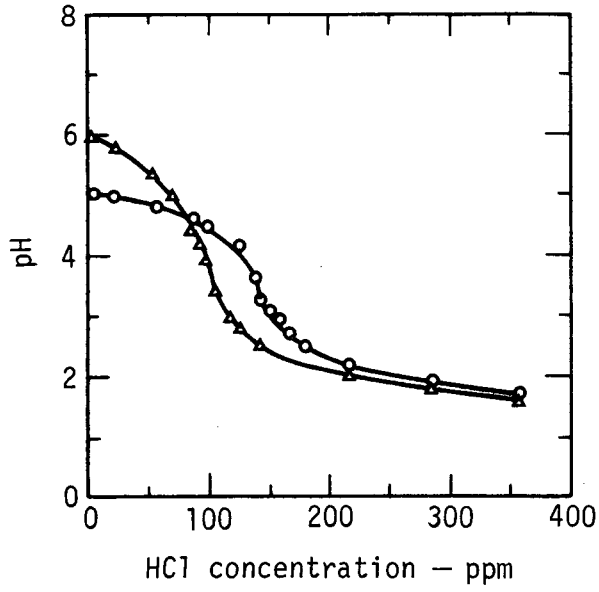

Fig. 21. Titration of geothermal brine with HCl: separated brine (Δ), sample No. LM-SB-TF91 and well-head brine (o), sample no. LM-BT-TF-90.

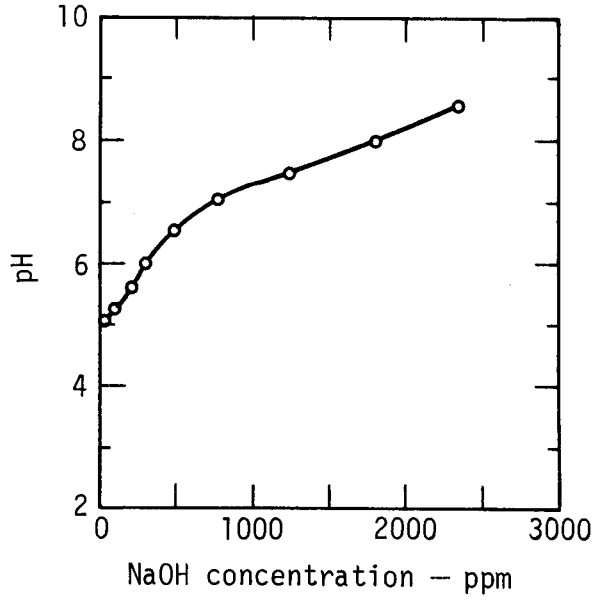

Fig. 22. Titration of geothermal brine with NaOH (sample No. LM-BT-TF-90).

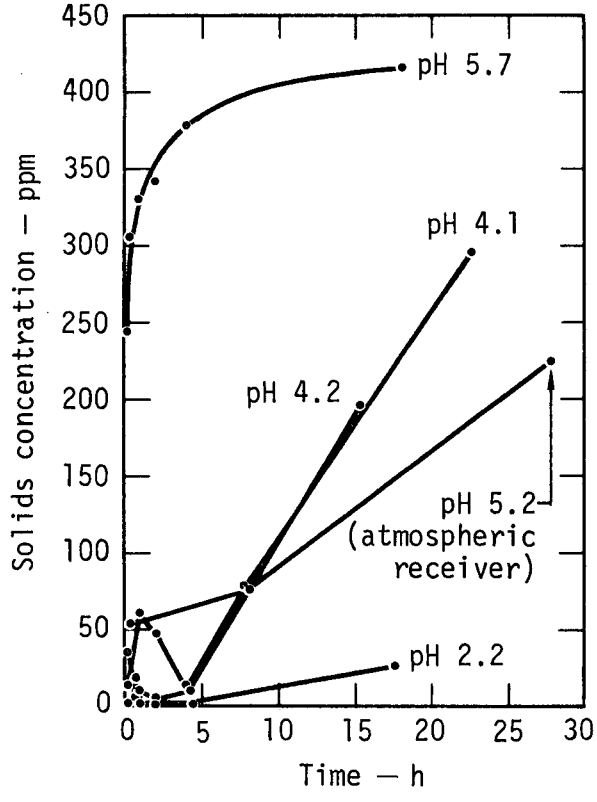

Fig. 23. Production of solids from geothermal brine at 85°C vs pH.

Previous experience shows that samples taken from the two-phase flow at the well head are rich in the liquid phase. Also, some NH_3 in the vapor phase of the wellhead sample may have been swept through the sampler, as noted above for the NH_3 in steam. Either of these sampling errors would give a negative bias to the acid consumption value of the wellhead sample when compared to the calculated value for whole brine.

A sample of wellhead brine was titrated with NaOH to determine the amount of base required to precipitate solids in the pH range from 5 to 8.5. The results (see Fig. 22) indicate that the addition of base to increase the pH of the brine to values greater than 6.0 probably is not economically attractive unless enough minerals can be recovered from the precipitated solids to offset the cost of the base.

The rate of formation of solids was determined as a function of pH for five samples of remixed brine that was flashed through nozzles in the LLL Total Flow Test Unit. For four samples, the liquid and vapor phases of the brine were first separated, acid was added to the brine, and then the brine and steam were remixed. One sample was taken from the atmospheric receiver. These samples were incubated in a water bath at 85°C for times ranging from 15 min to 26 h. The solids were filtered out on 5-μm glass filters, dried, and weighed. The results for solids production in the pH range from 2.2 to 5.7 are shown in Fig. 23. The results indicate that, in remixed brine acidified to pH $\leq$4.2, solids production is inhibited for at least 4 h. No data were obtained for samples taken from the atmospheric receiver in the interval from 0.5 to 8 h because the solids plugged the filters. Results shown for times greater than 8 h may show a positive bias because Fe^{2+} oxidizes to Fe^{3+} during digestion, allowing $Fe(OH)_3$ to precipitate.

Interest in the removal of solids from spent brine was revived recently following the plugging of the Magmamax No. 3 well by solids in the reinjected brine. Preliminary experiments were made to study the settling rates of suspended solids and methods to coagulate them. Three methods of brine treatment were screened. The first was simply to increase the pH by adding NaOH solution to accelerate the precipitation of silica and other materials. The other two methods of treatment were variations of the common water-treatment practice of adding a flocculating agent to speed settling and improve filterability. The first variation on this theme was to add ferric chloride and then NaOH solution to produce the flocculant ferric hydroxide.

The other method produced ferric ion from ferrous ion already present in the brine by adding an oxidant (e.g., NaClO in Chlorox bleach) and then precipitating solids with NaOH solution. The treated brine was placed in unthermostated 500-cm^3 graduated cylinders, observed visually, and sampled at the conclusion of the experiment.

As compared to untreated samples, all three methods of brine treatment increased the settling rate of the solids and visibly decreased the amount of suspended solids remaining in the supernate after settling. Visual observation of these experiments indicated that the best conditions for rapid settling and nearly complete clarification of the supernate require ferric ion concentrations from 10 to 50 ppm and precipitation at a pH of approximately 6. Under these conditions, the majority of the precipitates settled in 0.5 to 1 h. Also, the flocculant remaining in the supernate was easily removed by filtering through a glass-wool filter. Samples of the supernates and filtrates are being analyzed to provide the basis for a more complete evaluation of the effect of each treatment.

Evaluation of Materials by Electrochemical Techniques for Geothermal Applications

Responsible Personnel: J. E. Harrar, R. D. McCright,* and A. Goldberg*

Brief Description: Electrochemical measurement techniques are employed to screen materials for corrosion resistance in acidified, hypersaline geothermal brine. Specifically, the techniques are used to establish the effect of pH on corrosion rate; to investigate the protectiveness of scale; and to aid in characterizing the brine itself.

Status: Further work has been carried out† to establish the behavior of various materials in geothermal brine. The types of measurements described previously for the 1976 field tests were continued in the most recent series. Six Petrolite Model M-3010 recording-corrosion-rate instruments were used with six test cells, enabling simultaneous measurement of up to six different materials. Usually, two cells were operated in series at each of the three plant test stations.

Because of lower brine flow rates at two of the effluent test stations, all tests in this series were carried out at a lower rate (350 cm^3/min) than was used in 1976. At this reduced rate of flow, the cell volume is replaced every minute. As a result of the lower flow rate, temperatures also were somewhat lower, ranging from 86 to 98°C; specific temperatures depended on the station, the position of the cell, and the time of day. The electrodes of test material were exposed to the brine without preheating; each test run was 16 to 20 h in duration. In some of the runs, the E_h and pH were also monitored. However, most of the pH data were obtained from measurements by the plant operators of the cooled effluent brine taken from sampling points adjacent to the corrosion test cells.

The results of the corrosion-rate measurements are summarized in Fig. 24. The longer test duration in this series (16 to 20 h) is believed to have produced more meaningful data than the 1976 series. Figure 24 was constructed

---

*Metals and Ceramics Division, LLL

†See Ref. 1, p. 43.

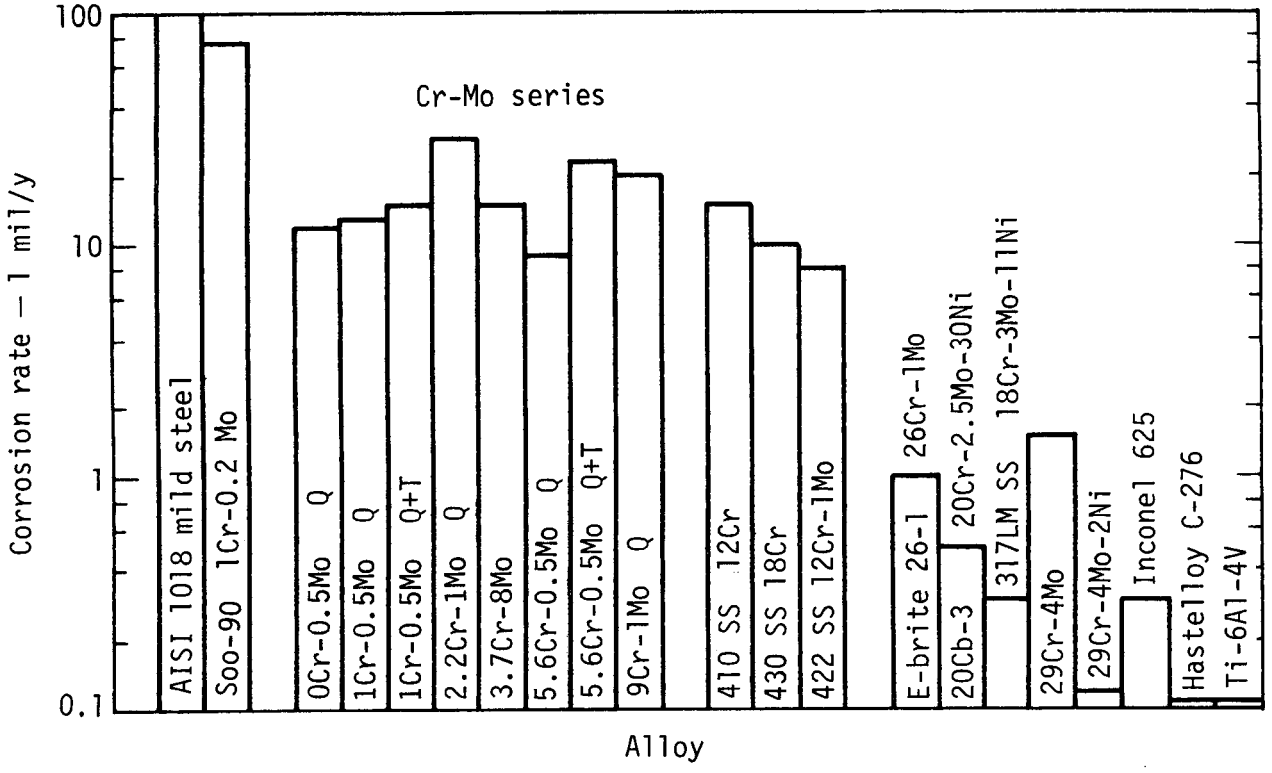

Fig. 24. Corrosion resistance of alloys in acidified geothermal brines at 86 to 98°C. LPR measurements were taken over 16- to 20-h tests: Q = quenched material and Q+T = quenched and tempered material.

from the corrosion rates observed during the last 2 h of each test. At that time, each material had reached a relatively stable corrosion rate which is believed to be most indicative of the material's long-term behavior.

The electrodes have not yet been examined for pitting corrosion, but on the basis of the observed typical corrosion rates, some tentative conclusions can be drawn:

- Generally, the behavior of these materials was the same as that observed in the 1976 tests. In this series, the pH control was tighter but again, there were no obvious correlations between corrosion rate and pH in the range of 2.0 to 4.5. However, it is now believed that measured corrosion rates will not accurately reflect pH variations of less than a few hours duration.
- The types 410, 422, and 430 stainless steels offer no advantage in general corrosion resistance over low-chromium/molybdenum alloys. The stainless steels also are more susceptible to pitting corrosion.
- Both the type 1018 mild steel and the Soo-90 (modified 4130) steels exhibit a steady, high corrosion rate of 75 to 100 mil/y in the acidified brine.
- No clear differences have yet emerged in the corrosion resistances of the Cr-Mo series, ranging from 0Cr-0.5Mo to the 9Cr-1Mo alloy. Even the 0Cr-0.5Mo alloy reached a corrosion rate of less than 20 mil/y after 10 h exposure. Further testing is required to reveal distinctions, if any, among different alloy compositions and heat treatments in this series. However, it is apparent that small amounts of chromium and molybdenum ($\geq$0.5%) significantly improve alloy corrosion resistance.
- Based on one experiment with the 5.6Cr-0.5Mo alloy, in which the same material was placed in two different cells in series, it appears that the reproducibility of measurement of the corrosion rates is approximately ±25%.
- From the behavior of the group of the resistant materials, it is evident that only the high-chromium, nickel-based, titanium-based, or chromium-nickel (e.g., 317LM SS) alloys are significantly better than those of the chromium-molybdenum series. The data also show that the addition of 2% nickel to the 29Cr-4Mo alloy improves the material's general corrosion resistance.

One experiment was conducted in which type 1018 mild steel was exposed first to pH 5.6 unmodified brine, and then to the acidified brine to observe the effect of prescaling on the corrosion rate. In 2 h of exposure to the unmodified brine, the corrosion rate dropped to about 4 mil/y and white scale (silica) growths were seen on the electrode. Upon acidification of the brine, the corrosion rate increased to approximately 40 mil/y and stabilized at this rate for the duration of the test. This corrosion rate is 2.5 times lower than that observed in the absence of scale (see Fig. 26). The white scale formations remained on the electrode during flow of the acid brine. This test again demonstrates the protective nature of the scale; however, we must note that the duration of the "acid" test still was relatively short.

Measurements also were made of the E_h of the separated brine. There appeared to be no significant change from the +0.20 ± 0.10 V vs the standard hydrogen electrode value found in 1976. Corrosion potentials were determined for the materials tested; these correlated very well with the measured corrosion rates. The values of corrosion potential for the chromium-molybdenum series were only slightly more positive than those of the mild steel and Soo-90, indicating little danger from galvanic corrosion if alloys from these two classes of materials are coupled together.

Numerical Studies of Combustion Processes

Responsible Personnel: J. R. Creighton

Brief Description: Detailed computer calculations of chemical kinetics and a simple mathematical model explain the growth of OH radical concentrations to well above equilibrium levels in the late stages of hydrocarbon oxidation. The high concentration of OH is important because it leads to pollutant formation in internal combustion engines.

Status: Both experiments and detailed computer calculations have shown that the concentration of radical species, especially OH, is at least ten times greater than the equilibrium concentration in the late stages of hydrocarbon combustion in an internal combustion engine. This large concentration contributes to the production of nitrogen oxides, a major pollutant. Computer calculations involving 20 chemical species and 45 elementary reactions for methane combustion have been performed. Analysis of the results explains the large concentration of OH.[20]

The rate constant for the reaction of OH with methane is large; thus, the concentration of OH remains low until nearly all of the methane is consumed. The same is true for any other hydrocarbon fuel because the rate constants are similar. Calculations indicate that when nearly all of the methane has reacted, CO begins to oxidize by the reaction,

$$CO + OH \rightarrow CO_2 + H \ . \qquad (1)$$

The H atoms then react with O_2:

$$H + O_2 \rightarrow OH + O \ , \qquad (2)$$

and the O atom concentration rises until O begins to react with H_2O:

$$O + H_2O \rightarrow 2OH \ . \qquad (3)$$

---

20. J. R. Creighton, Some General Principles Obtained from Numerical Studies of Methane Combustion, Lawrence Livermore Laboratory, Rept. UCRL-78849 (1977).

The concentrations of O and H reach levels where the rates of reactions (1), (2), and (3) are all equal. Thus, the concentration of OH rises exponentially:

$$[OH] \rightarrow A \exp \{2 k_1 [CO] (t - t_0)\} \quad . \tag{4}$$

The coefficient A is the concentration of OH at time t_0, the instant when all of the methane is consumed. The factor k_1 is the rate constant for reaction (1). Also, [CO] is the molar concentration of CO and it remains nearly constant as the radical concentrations change. The growth of the radicals is illustrated in Fig. 25.

Both computer calculations and a simple mathematical model show that the concentrations of O and H rise in proportion to OH but remain much smaller. Eventually, the radical concentrations rise to the point where the following reaction becomes important:

$$H + OH + M \rightarrow H_2O + M \quad . \tag{5}$$

Here, M represents the sum of the concentrations of all species which act as a third body in reaction (5).

Once reaction (5) becomes important, all of the radical concentrations become more or less constant. The rates of reactions (2), (3), and (5) are all approximately equal at one-half the rate of reaction (1); see Fig. 26. The maximum OH concentration is therefore

$$[OH]_{max} \rightarrow k_2 [O_2]/k_4 [M] \quad . \tag{6}$$

This concentration is at least ten times greater than the equilibrium concentration of OH and contributes to the generation of the nitrogen oxides. Calculations show that after nearly all of the CO is gone, recombination reactions bring the radical concentrations down to the equilibrium value.

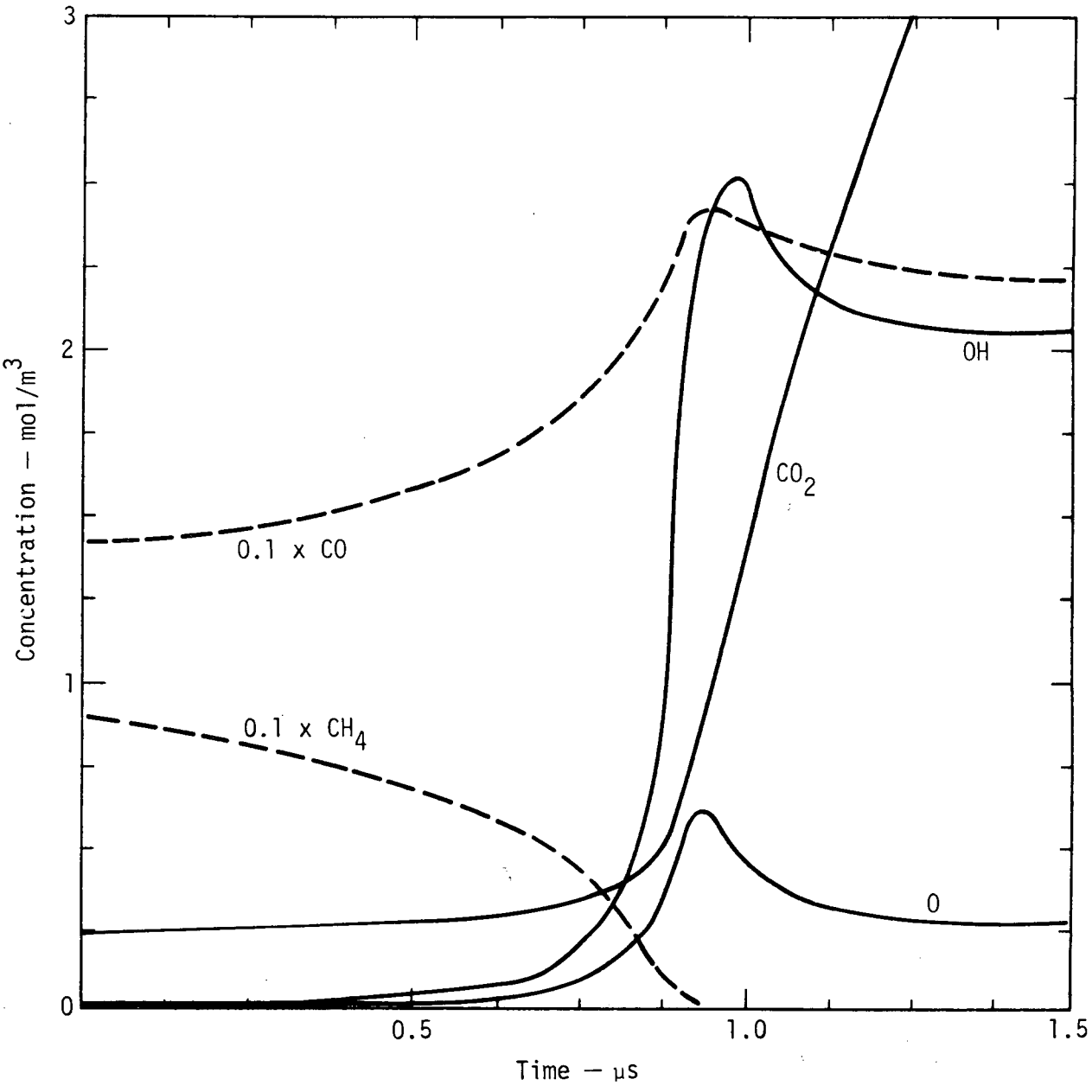

Fig. 25. Concentration of species in methane combustion. Methane is oxidized to CO but further oxidation to CO_2 is minimal until methane disappears. The concentrations of O and OH are increased and new steady state concentrations are reached. The higher concentrations of OH react with CO to form CO_2 at a more rapid rate. The zero point in time was chosen arbitrarily so that changes appear on an approximate scale.

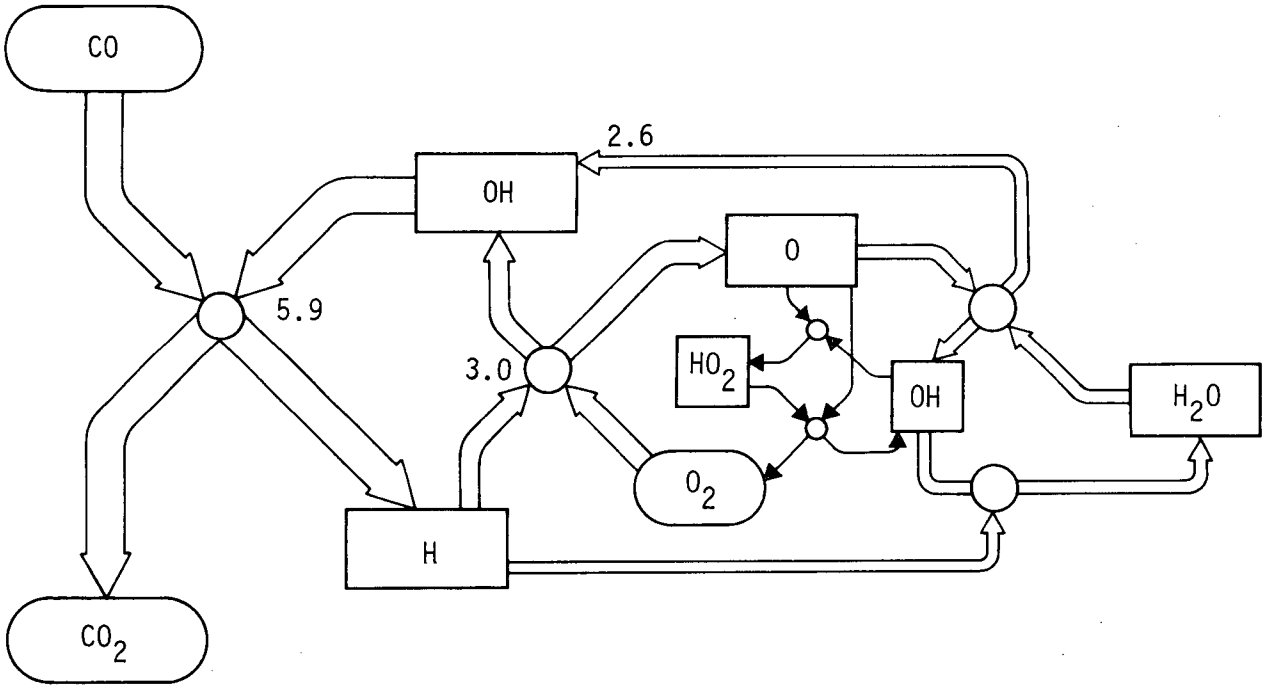

Fig. 26. Reactions involved in the oxidation of CO in the late phases of methane combustion. The circles represent reactions and arrows represent reactants and products. The width of the arrows is proportional to the relative rates of reactions and numerical values of some relative rates are shown. A few other reactions, not shown, contribute about 10% to balance the reaction rates.

Special Projects

A Direct-Reading Emission Spectrometer for the NURE Program

Responsible Personnel: E. S. Peck and A. L. Langhorst, Jr.*

Brief Description: A direct-reading emission spectrometer system has been purchased and installed for use in the National Uranium Resource Evaluation (NURE) Program to analyze water and sediment samples.

Status: A Jarrell-Ash 0.75-m "AtomComp" spectrometer system has been installed in Building 281. Both an inductively-coupled argon plasma (ICAP) source and a constant-current dc-arc source are associated with the spectrometer. The system is controlled by a PDP-8/e central processing unit (CPU). The CPU handles many of the experimental parameters and provides data output and manipulation. Preliminary check-out tests have been completed and calibration will be undertaken soon. The system will be used first for the analysis of water samples for the NURE program.[21] These analyses will be performed using the ICAP source.

The ICAP source is powered by an rf generator that delivers up to 2 kW of power at 27.13 MHz through a water-cooled inductance coil. The coil surrounds the top of a quartz torch assembly through which the nebulized sample is carried in flowing argon. An adjustable pi network matches the output impedance of the power supply to the argon gas discharge.

Radiation from the plasma, defined by the spectrometer entrance slit, is dispersed by the grating and falls on specific exit slits. The light that passes through each exit slit is transduced by a photomultiplier into an electronic signal which is detected by the CPU. The dc arc source operates in a conventional manner and is similar to the source currently in use in the General Chemistry Division spectrographic section. The radiation from this source is handled in the same manner as that for the ICAP. This source will be used to analyze powdered sediment samples.

---

*Environmental Sciences Division, LLL.

21. General Chemistry Division Quarterly Report, April through June 1975, Lawrence Livermore Laboratory, Rept. UCID-15644-75-2 (1975), p. 26.

In its current configuration, the system contains 44 channels (each exit slit and its associated photomultiplier is called a channel). Of these, 40 are analytical channels, three are background channels, and one is a mercury alignment channel. The analytical channels cover 26 elements, one of which (Ge) is designated as the internal standard channel for the dc arc source. This configuration is designed to determine concentrations of Al, As, Ca, Cd, Co, Fe, K, Li, Mg, Mo, Na, Ni, P, Si, U, V, and Zn in water samples and Al, Ca, Ce, Co, Cu, Fe, K, La, Mg, Mn, Mo, Na, Ni, Pb, Si, Ti, U, V, Y, Zn, and Zr in powdered samples. Expected detection limits for the elements in water samples are below 1 ppm. Similar limits for powdered sediments range from 1 to 5000 ppm.

Laser Spectroscopy of Atoms: Accurate Ionization Potentials from Rydberg Series in Lanthanides

Responsible Personnel: E. F. Worden, R. W. Solarz,* J. A. Paisner,* L. R. Carlson, and J. G. Conway†

Brief Description: Laser spectroscopy techniques have enabled us to obtain Rydberg series in several lanthanides. From the series limits, the following ionization limits (in electron volts) were accurately determined: Ce, 5.5387; Nd, 5.5250; Sm, 5.6437; Eu, 5.6704; Dy, 5.9390; Ho, 6.0216; and Er, 6.1074. With the exception of Eu, these limits are 10 to 100 times more accurate than the previous experimental values. This work is part of the laser isotope separation studies being carried out in Y-Division.

Status: Using laser spectroscopy techniques, the detection of Rydberg series in atoms with complex spectra (e.g., uranium) has been demonstrated at LLL.[22] Several similar techniques have been used to determine Rydberg series in several lanthanides. The apparatus and excitation techniques are similar to those described previously.[22,23] In place of the CO_2 radiation used previously to ionize the populated Rydberg levels, field ionization and collisional ionization were used for Ce and Ho to observe Rydberg series converging to the ground state of the ion.

The series observed for Ce is shown in Fig. 27. The ionization limit is determined from the series by plotting the quantum defect n-n* vs n for various assumed limits as shown in Fig. 28. The limit giving the smoothest and most constant quantum defect plot is chosen as the correct limit for the element. The value of n* (the effective quantum number) is obtained from the formula

---

*Y-Division, LLL.

†See Ref. 1, p. 22.

22. R. W. Solarz, C. A. May, L. R. Carlson, E. F. Worden, S. A. Johnson, J. A. Paisner, and L. J. Radziemski, Phys. Rev. A14, 1129 (1976).

23. R. W. Solarz, J. Opt. Soc. Am. 66, 846 (1976).

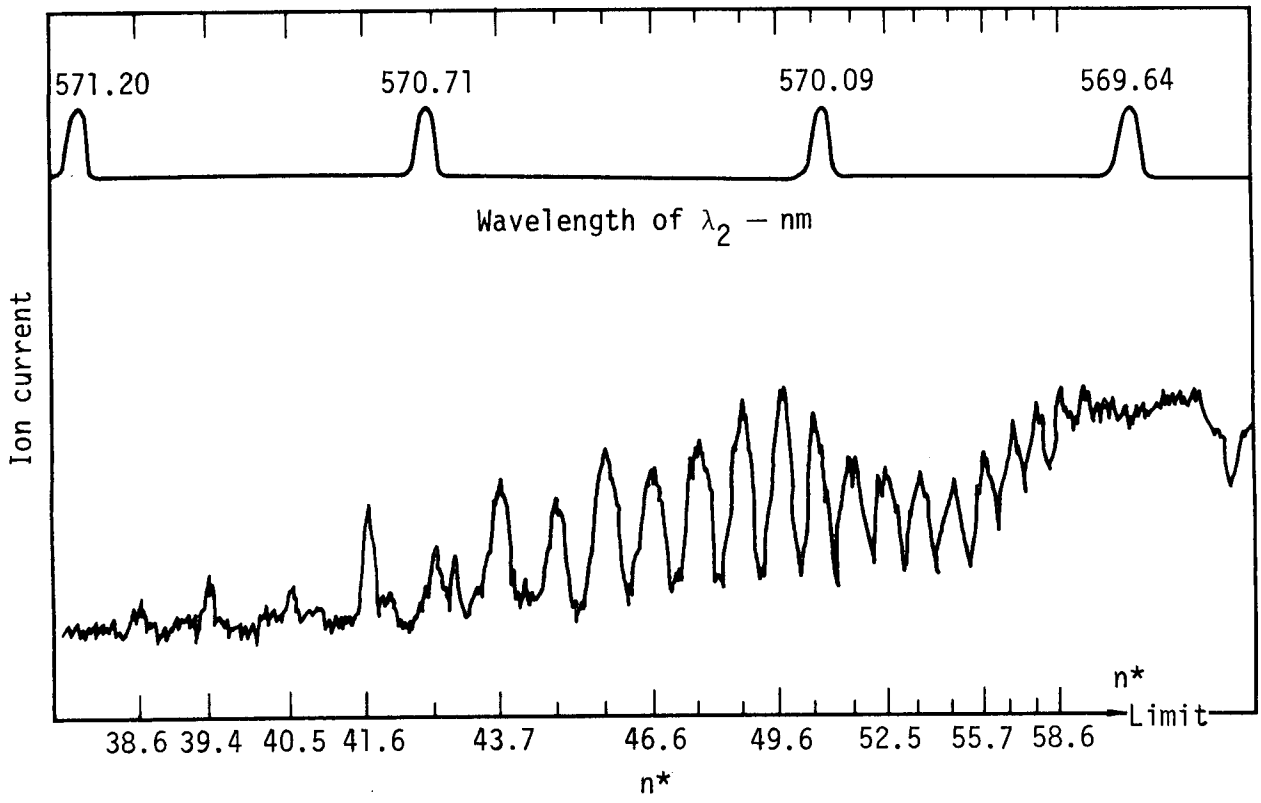

Fig. 27. Ryberg series for Ce converging to the ground state of the ion was obtained by field ionization of levels populated by λ_2 in a two-step process. The field ionization pulse was delayed 4 μs. Primary excitation was to the 27091.56 cm^{-1} level by λ_1 at 387.3 nm (1279 to 27091 transition). Series limit is at 568.69 nm (not shown).

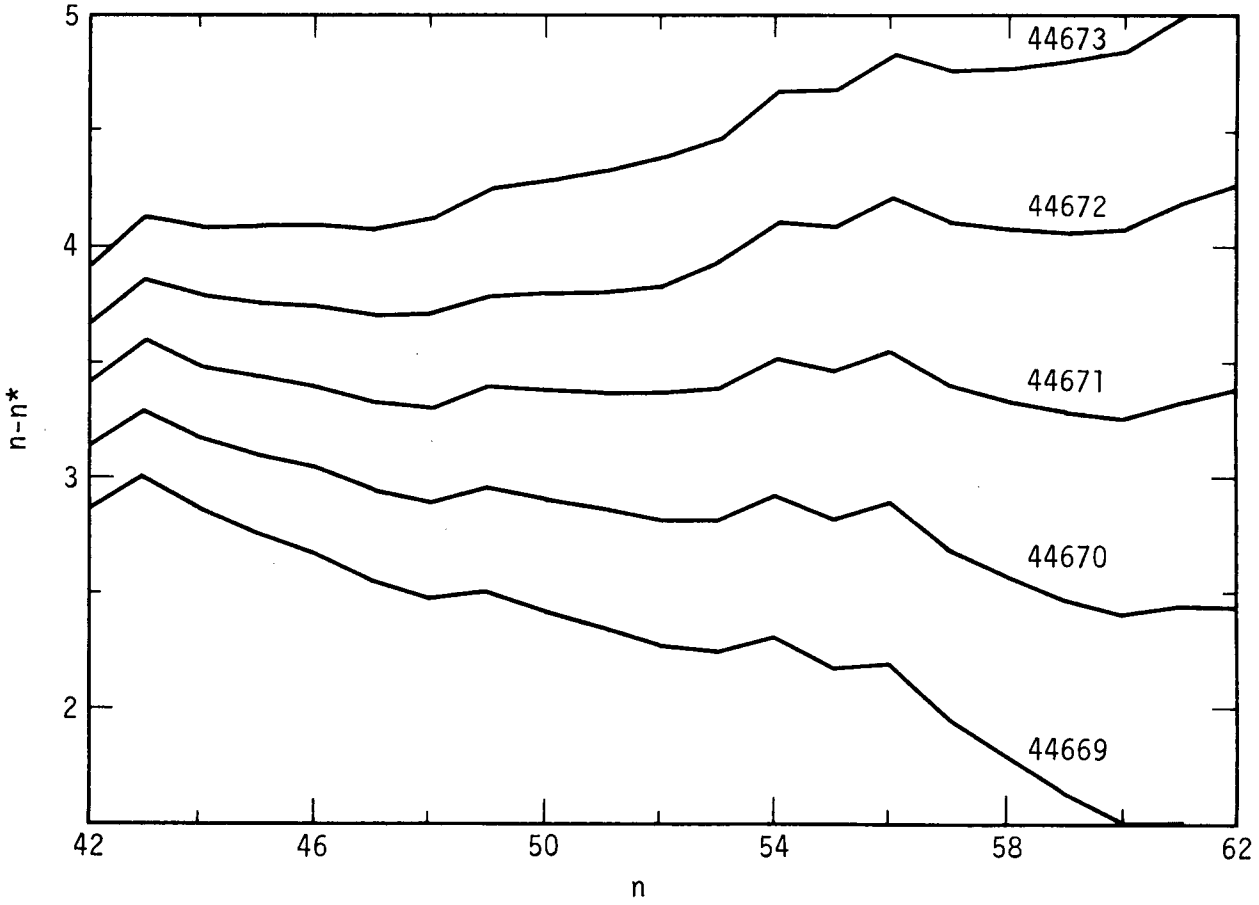

Fig. 28. Quantum defect plot for Ce Ryberg series for various assumed limits. Levels used are those from Fig. 6.

$$n^* = [R/(\text{limit} - \text{level value})]^{1/2} ,$$

where R is the Rydberg constant. Autoionizing Rydberg series were observed for Nd, Sm, Eu, Dy, and Er. These series converge to the excited levels of the ion. The levels of the observed series occur at energies above the first ionization limit (limit converging to the ion ground state) indicating that they are autoionizing levels. The convergence limit value is obtained by the technique described above. The ionization limit is obtained by subtracting the energy of the ion level. Agreement of this value with the less accurate value obtained from the photoionization threshold is always determined first so that we can calculate the wavelength range in which to search for Rydberg levels.

The values obtained are given in Table 8. The spectroscopic data, wavelengths, and levels used to obtain the limits were determined from Ref. 24 with the exception of the second excited level used for Ho. This level was determined by techniques described in Ref. 23, necessary because of the lack of known levels in this energy range.

Table 9 is a comparison of our results with those obtained by other methods. With a few exceptions, the values agree to within the error limits stated for each method. The surface ionization and electron impact values for Ho and Er appear low. The spectroscopic values for Ce, Pr, and Ne are low. This may reflect the inaccuracy of the extrapolation technique used for values near the beginning of the series.

In general, our values are 10 to 150 times more accurate than values reported to date. Our value for Eu compares very well with the value obtained by Smith and Tomkins[25] from a long series observed in absorption with a high-resolution spectrograph. Accurate limits have been obtained for Tm, Yb, and Lu by Camus and Tomkins[26,27] by the absorption method. We plan to observe the Gd and Tb limits using our technique and, with the exception of Pm, this will complete the series.

---

24. W. F. Meggers, C. H. Corless, and B. F. Scribner, Tables of Spectral-Line Intensities, Part I, N.B.S. Monograph 145 (U.S. Government Printing Office, Washington, D. C., 1975).

25. G. Smith and F. S. Tomkins, Proc. Roy. Soc. (London) A342, 149 (1975).

26. P. Camus and F. S. Tomkins, J. Phys. (Paris) 30, 545 (1969).

27. P. Camus, Thesis, University of Paris, Orsay (1971), pp. 181-265.

Table 8. Lanthanide Rydberg series limits[a]

Element	λ_1, A	λ_2,[b] A	Excited Level Used, cm^{-1}	Convergence Energy, cm^{-1}	Convergence Level in Ion, cm^{-1}	First Ionization Limit,[c] cm^{-1}	First Ionization Limit,[c] eV
Ce	3793.83	—	26331.11	44674(3)	0.00	44674(3)	5.5389(4)
	3873.03	—	27091.56	44671(3)	0.00	44671(3)	5.5385(4)
Nd	4924.53	—	20300.84	45075(5)	513.32	44562(5)	5.5250(6)
Sm	4596.74	—	22041.02	45846(8)	326.64	45519(8)	5.6437(10)
Eu	4594.03	—	21761.26	47403(2)	1669.21	45734(2)	5.6703(3)
	4661.88	—	21444.58	47405(2)	1669.21	45736(2)	5.6706(3)
	6291.34	6787.48	30619.49	47403(2)	1669.21	45734(2)	5.6703(3)
Dy	4211.72	—	23736.60	48730(5)	828.31	47902(5)	5.9391(6)
	6259.09	6769.79	30739.79	48727(5)	828.31	47899(5)	5.9388(6)
Ho	4103.84	—	24360.55	49203(5)	637.4	48566(5)	6.0215(6)
	6305.36	6947.1	30246 ±2	48567(5)	0.00	48567(5)	6.0216(6)
Er	6221.02	6451.56	31565.94	49699(5)	440.43	49259(5)	6.1074(6)

[a] Wavelength and energy levels obtained from Ref. 4 and the references therein. Number in parentheses is the uncertainty in the last digit.

[b] No value of λ_2 is given for two-step observations when λ_2 is scanned. Values given are λ_2 for three-step observations.

[c] To convert values from cm^{-1} to eV, multiply by 8065.479 cm^{-1}/eV.

Table 9. Comparison of first ionization potentials of some lanthanides obtained by various techniques.

Element	Ionization potential, eV					
	Surface ionization,[a] Ref. 28	Electron impact,[a] Ref. 29	Ref. 30	Spectroscopic extrapolation, Ref. 31	Laser photoion onset, this work	Rydberg convergence, this work
Ce	5.54	—	5.44	5.47(5)	5.537(4)	5.5387(4)
Pr	4.50	—	5.37	5.42(3)	5.464(5)	—
Nd	5.49	—	5.49	5.489(20)	5.523(3)	5.5250(6)
Sm	5.61	5.56	5.58	5.63(3)	5.639(3)	5.6427(10)
Eu	5.64	5.61	5.68	5.67(1)	5.666(3)	5.6704(2)[b]
Dy	5.82	5.8	5.90	5.93(5)	5.936(3)	5.9389(6)
Ho	5.89	5.85	5.99	6.02(5)	6.017(3)	6.0216(6)
Er	5.95	6.11	5.93	6.10(8)	6.104(3)	6.1074(6)

[a] Error limits are given as ±0.1 eV for all values.

[b] A value of 5.67045(3) eV has been obtained by Smith and Tomkins[18] from a long Rydberg series observed in absorption.

28. G. R. Hertel, J. Chem. Phys. 48, 2053 (1968).

29. K. F. Zmlov and J. L. Margrave, J. Phys. Chem. 70, 3014 (1966).

30. R. J. Ackermann, E. G. Rauh, and R. J. Thorn, J. Chem. Phys. 75, 1027 (1976).

31. W. C. Martin, L. Hagan, J. Reader, and J. Sugur, J. Phys. Chem. Ref. Data 3, 771 (1974) and references therein.

Microwave-Spectrometer Multiple-Gas Analyzer

Responsible Personnel: L. W. Hrubesh, R. L. Morrison, A. S. Maddux,* J. N. Nielson,* and M. L. Malachowsky†

Brief Description: We have undertaken a study to develop and construct a microwave spectrometer that will be able to monitor ten gases — acetonitrile, methyl alcohol, ethyl alcohol, iospropyl alcohol, acetaldehyde, carbonyl sulfide, sulfur dioxide, ethylene oxide, and acetone — at the part-per-million level in air.

Status: The General Chemistry Division has obtained a contract from the National Institute of Occupational Safety and Health (NIOSH) to develop and fabricate a portable microwave spectrometer to monitor the above ten gases at the part-per-million level in air. The instrument has the following specifications:

- The instrument will be designed for minimum size and weight and will be sufficiently rugged for field use. We are striving for a size under 0.056 m^3 (2 ft^3) and a weight less than 77 kg (35 lb).
- Emphasis will be placed on minimum power requirements.
- The instrument will use a varactor-tuned Gunn oscillator as a source of microwave power.
- Frequency stabilization for the microwave power source will be achieved by locking onto a resonance line of a reference gas sample.
- The inlet system to the sample cell will employ a permselective membrane as a sample preconcentrator.
- The sample cell will be a shortened waveguide Stark cell operating in the R-band.
- An electronic capability for a field calibration check and a procedure for precise laboratory calibration will be provided.

During the first quarter of development, we have clarified and defined the design concepts for the electronics, vacuum system, and inlet system for an operating breadboard instrument. To reach the final electronic design, we performed two brief studies.

---

*Electronics Engineering Department, LLL.

†Mechanical Engineering Department, LLL.

The first of these studies was to determine the sensitivity of a bolometer as a detector for the spectrometer. This study was motivated by the desire to reduce the modulation frequency for the spectrometer so that very simple and compact high-voltage Stark modulators could be used. The bolometer does not have an inverse frequency noise component typical of the diode detectors. For this reason, bolometers often have been used successfully when low-frequency modulation is required. However, for our purposes, we could not give up sensitivity for compactness.

Our study was mainly empirical. We made a direct comparison of the signal/noise ratio between a diode detector and a properly biased bolometer as a function of modulation frequency with a constant concentration of gas in our Stark cell. The results conclusively showed that a greater sensitivity was available with the diode detector. This was true even at higher incident microwave power levels where the diode becomes a linear detector and the bolometer should have a signal/noise ratio advantage. Although there is a considerable variability between diodes and probably also between bolometers, we conclude that no significant overall advantage would be gained by using a bolometer detector. Therefore, we will use a broadband diode detector for the NIOSH instrument.

A second study determined the feasibility of combining several permeation sources in a single container to supply reference gas signals. We determined that it will be possible to have two sets of five chemically compatible compounds, each with sufficiently isolated absorption lines. There is no evidence that, within these two sets of compounds, chemical reactions which degrade the reference signal will occur. From the measured permeation rates, we estimated that the minimum lifetime for any of the tubes will be one month of continuous operation.

We also developed techniques to adjust the permeation rates of all compounds so that each compound has nearly the same absorption intensity in the reference cell. This will considerably simplify our electronics for the search-lock mode. In addition, we tested the necessary experiment to determine whether or not any of the ten reference gases would react with each other in the Stark reference cell. These experiments have led us to the conclusion that, at 8 Pa and in a dry environment, none of the gases will react.

We also are testing a circuit to provide automatic gain control in the search-lock operation for frequency stabilization. This circuit will provide sufficient gain for a stable frequency lock onto each of the reference lines, regardless of their intensity variations. Such a circuit also will ensure a stable lock under conditions that might change the line intensity (e.g., variable vacuum pump characteristics).

During the next quarter, we intend to complete the fabrication of an operating breadboard instrument and to begin testing our design concepts.

Experimental Demonstration of the Effects of Turbulence and Electric Fields on Coagulation Processes of Aerosols

Responsible Personnel: M. M. Fulk and E. B. Huss

Brief Description: Aerosol generators have been built and assembled to produce various aerosols ranging in size from 0.01 to 1.0 μm in diameter. An electrical aerosol-size analyzer which counts and sizes aerosols ranging in diameter from 0.003 to 1.0 μm is operational. We are developing methods to observe coagulation processes in these aerosols in real time.[32] The hypergolic approach thus far has been disappointing. However, the chemiluminescent approach has shown some immediate promise.

Status: A high-temperature aerosol generator has been built. It can produce, for example, particles of NaCl 0.01 μm in diameter at a concentration of 10^6 particles per cubic centimeter. These particles can be used either directly or as condensation nuclei on which a second material can build to produce aerosols of controlled size and number.

A second generator also was built to condense pentaerythritol tetranitrate (PETN) onto these NaCl nuclei, producing PETN particles 0.1 to 0.2 μm in diameter. (This generator required that additional safety structures be built around the apparatus.) Also, as reported earlier, an ultrasonically driven liquid droplet generator is operational.

We have assembled and operated an electrical aerosol-size analyzer (Thermal Systems Inc. Model 3030) to count and size particles with diameters ranging from 0.003 to 1.0 μm. This size region is difficult to measure. However, it is essential that we be able to do so because the majority of debris particles fall into this size range. In addition, it is important that the coagulation dynamics of these particles be studied.

We are developing methods to "see," in real-time, the processes of coagulation of these small aerosol particles with larger water droplets (10 to

---

32. General Chemistry Division Quarterly Report, April through June 1976, Lawrence Livermore Laboratory, Rept. UCID-15644-76-2 (1977), p. 28.

50 μm in diameter). Two approaches are being actively considered. The hypergolic approach thus far has been disappointing. However, the chemiluminiscent approach has shown some immediate promise.

In the first rough experimental run, approximately 10^{-11} g of Fe(II) could be seen easily in a single event. Single 10^{-3}-cm^3 drops of 5×10^{-5} M Fe(II) were introduced onto the surface of a "large drop" of second solution (5×10^{-3} M sodium luminol, 0.1 M KOH, 0.1 M boric acid, and 0.02 M H_2O_2) contained in a petri dish on the face of a photomultiplier (PM) tube. The small drops were introduced, one at a time, at various speeds ranging from about 0.1 to 30 cm/s. When the two drops collided, the system emitted light. The PM tube (RCA type 7265, operating at 2500 V) yielded a 500-mV signal with a rise time of about 10^{-5} s and a duration of approximately 10^{-3} s. The PM tube noise at operating conditions was only a few millivolts.

Each microlitre drop contained 2.8×10^{-9} g of Fe(II). In these experiments, it appears that we can "see" about 10^{-11} g of Fe(II) per event. We expect to be able to tune this approach to obtain still greater sensitivity.

PLL/gw/vt